CHAPTER 6: SPECIAL MONITORING STUDIES & DATA ANALYSES ASSOCIATED WITH THE IMPROVE PROGRAM

The results of four special studies conducted in association with the IMPROVE program are summarized here. The Big Bend Regional Aerosol and Visibility Observational (BRAVO) study is summarized in section 6.1 with details available in the full report available at http://vista.cira.colostate.edu/improve/Studies/BRAVO/Studybravo.htm and in associated journal articles. The Yosemite Aerosol Characterization Study (YACS) is summarized in section 6.2, details can be found on the web at http://vista.cira.colostate.edu/improve/Studies/YACS/studyYACS.htm and in associated journal articles. Section 6.3 summarizes the findings from the review of the improve equation for estimating ambient light extinction coefficients, the details are available in the full report at http://vista.cira.colostate.edu/improve/Publications/GrayLit/016_IMPROVEeqReview/IMPROVEeqReview.htm and in associated journal articles. The results of a coarse mass speciation study are included in section 6.4.

6.1 EXECUTIVE SUMMARY: BIG BEND REGIONAL AEROSOL AND VISIBILITY OBSERVATIONAL (BRAVO) STUDY RESULTS: AIR QUALITY DATA AND SOURCE ATTRIBUTION ANALYSES RESULTS FROM THE NATIONAL PARK SERVICE / COOPERATIVE INSTITUTE FOR RESEARCH IN THE ATMOSPHERE

Big Bend National Park is located in southwestern Texas along the Mexican-Texas border (Figure 6.1). During the 1990s, the haze at Big Bend and other sites in west Texas and southern New Mexico increased, further obscuring Big Bend's and nearby regions scenic beauty. In response to the increased haze, the Big Bend Regional Aerosol and Visibility Observational (BRAVO) study was conducted. This was an intensive monitoring study sampling aerosol physical, chemical, and optical properties, as well atmospheric dispersion using synthetic tracers from July through October 1999. The monitoring was followed by a multiyear assessment of the causes of haze in Big Bend National Park, Texas, with the primary purpose to identify the source regions and source types responsible for the haze at Big Bend. Secondary research objectives of the study were to learn more about the chemical, physical, and optical properties of aerosols responsible for haze. BRAVO study participants include the National Park Service (NPS), the U.S. Environmental Protection Agency (EPA), the Texas Commission on Environmental Quality (TCEQ), and the Electric Power Research Institute (EPRI), among others.

In support of BRAVO, the NPS and Cooperative Institute for Research in the Atmosphere (CIRA) at CSU analyzed the measured aerosol data to better understand the chemical, physical, and optical properties of Big Bend's haze, and conducted a number of complementary qualitative and quantitative haze source apportionment analyses. All source apportionment techniques went through extensive validation and evaluation tests and only those techniques which passed these tests were applied to Big Bend's haze. In addition to the analysis of the BRAVO study data, long-term Big Bend air quality and meteorological data were analyzed to determine the representativeness of the BRAVO time period to other seasons and years.

This Executive Summary summarizes the key findings from the analyses and their implications concerning Big Bend's haze with a focus on the apportionment of particulate sulfate and its contribution to Big Bend's haze. The body of this technical report provides detailed descriptions of the methods, evaluation and validation procedures and results from the multiple analyses employed by the NPS/CIRA group and the reconciliation between all source attribution techniques.

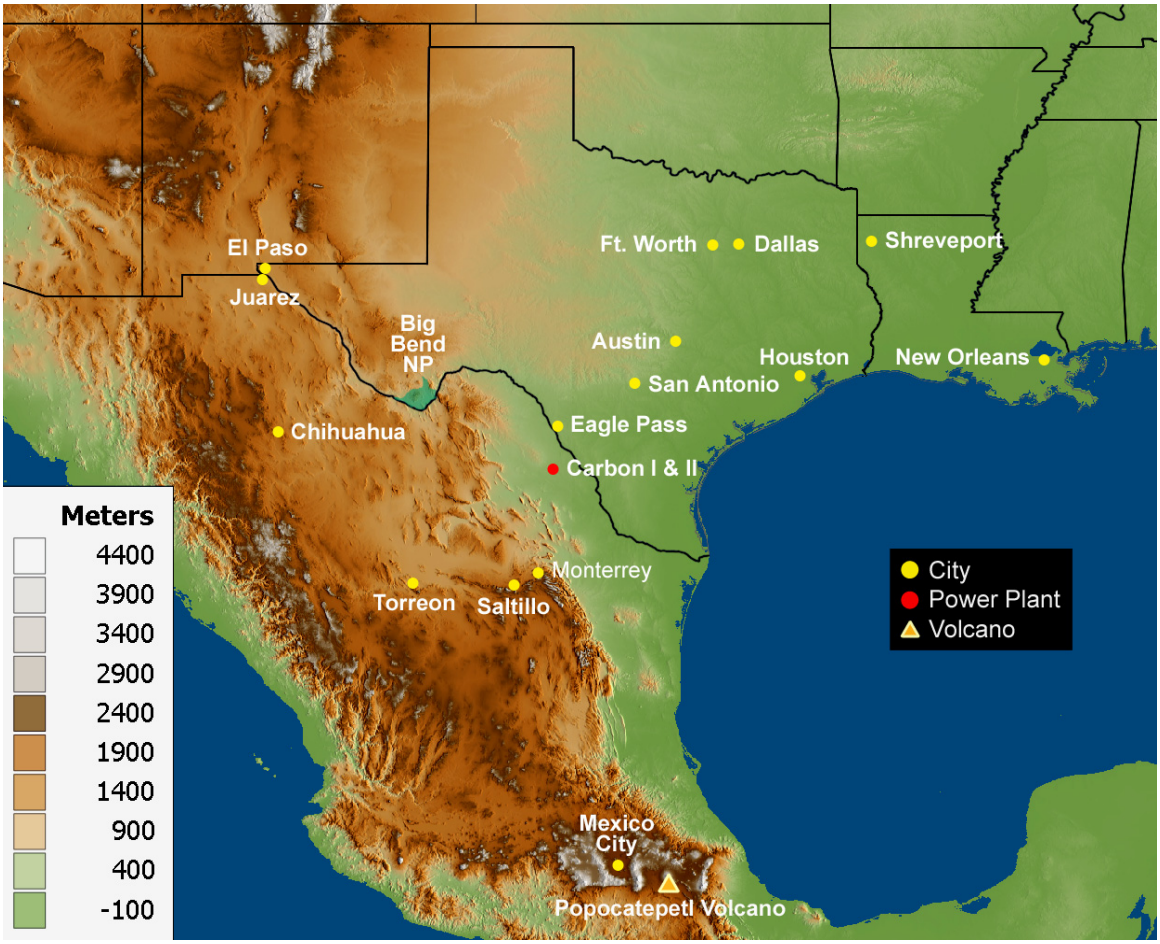

Figure 6.1. A terrain map of Texas and Mexico as well as some major cities and points of interest from the BRAVO study.

6.1.1 Characterization of Big Bend's Haze

Haze is caused by scattering and absorption of light by suspended fine liquid or solid particles in ambient air, known collectively as atmospheric aerosol. The sum of the light scattering and absorption is known as the light extinction and can be thought of as the fraction of light lost per unit of distance. The units of light extinction are inverse distance, e.g., 1/(million meters) or Mm^{-1}. Higher light extinction levels correspond to hazier conditions.

Detailed particle size and chemical composition measurements made at Big Bend during the BRAVO study were used to develop advanced estimates for each day's contributions to light extinction by the major aerosol components. These compare well to direct optical measurements of light scattering and light extinction. Figure 6.2 shows the daily particulate light extinction (sum of light scattering and absorption) contributions by the major aerosol components. As shown, there is a distinct difference in the particulate extinction budget in the first and second half of the BRAVO study. From July 1–August 15, the light extinction is primarily due to ammoniated sulfates (35%), organics (20%), and coarse mass (30%). In the second half of the study, post-August 15, the ammoniated sulfates account for 50% of the particulate extinction

while organics and coarse mass each account for about 20%. On the haziest 1/5th of the days, sulfate compounds accounted for about 55% of the particulate b_{ext} and organics 15%.

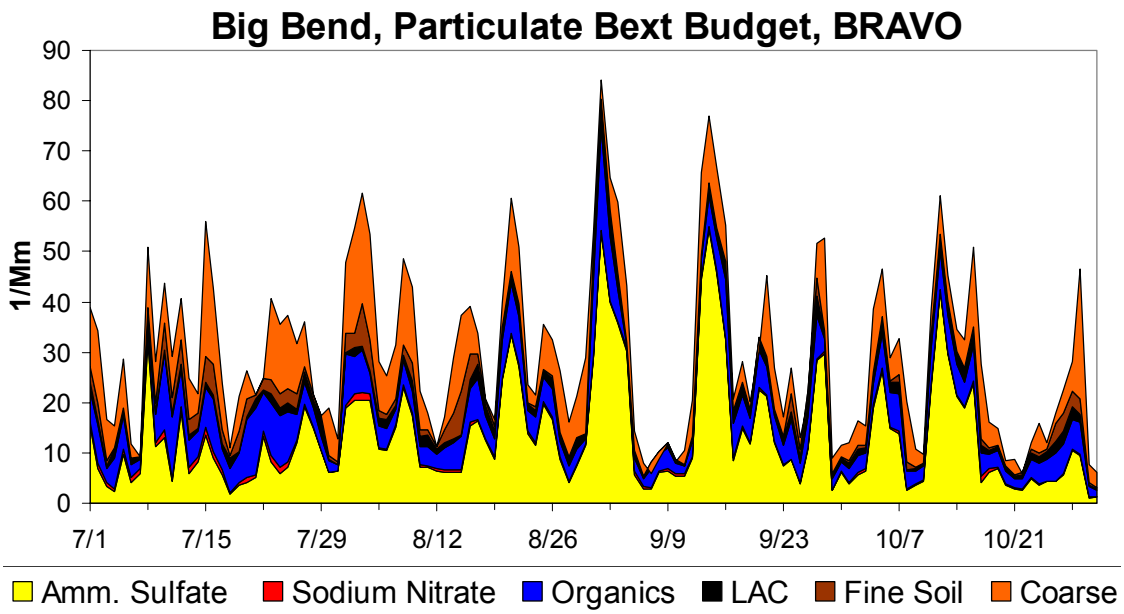

Figure 6.2. Big Bend's particulate light extinction budget during BRAVO.

The BRAVO period can be put into a larger climatological context by examining Big Bend's extinction budget over a long time period. Figure 6.3 shows the five-year (1998 through 2002) light extinction budget from measurements made every three days at Big Bend National Park in the IMPROVE monitoring network. In general, there are two periods of high haze at Big Bend National Park – one in spring when particulate sulfate and carbonaceous compounds contribute in similar amounts to haze and another in late-summer/fall when particulate sulfate compounds are the largest contributors to haze. Similar to the BRAVO period, the particulate sulfate compounds usually contribute more to haze than any other individual aerosol component. Carbonaceous particulate matter – organic compounds and light absorbing carbon (LAC) – generally constitute the second largest individual aerosol component contributing to haze at Big Bend National Park and on some days are the single largest contributor to haze. Information from other studies shows that during late spring episodes, concentrations of carbonaceous compounds are increased due to biomass burning in Mexico and Central America. Dust, represented by a combination of fine soil and coarse mass, contributes as much to haze as particulate sulfate compounds during the months of March and April.

On average, sulfate compounds contribute more to light extinction on the haziest days (53%) than for average days (48%). The contribution of carbonaceous (i.e., organic and light absorbing carbon) compounds to light extinction remained the about the same at 23% on average and the haziest days. The coarse mass is also a major contributor to the particulate light extinction, accounting for about 17% of the particulate light extinction on average and 15% on the haziest days. Since the sulfates accounted for more than half of the particulate extinction on the highest haze days, the lower contribution of organics and the fact that they have a potentially large contribution from smoke and other natural sources lead us to concentrate on understanding the source attribution of sulfate.

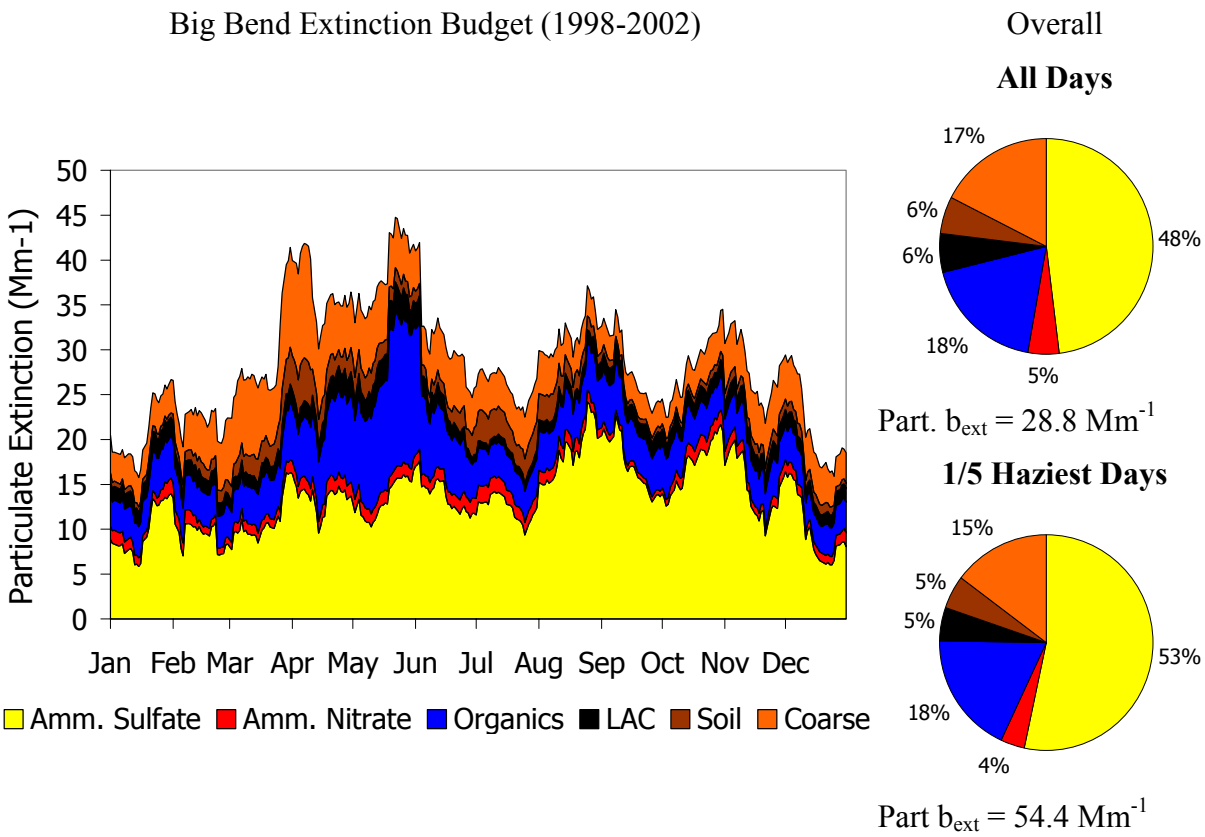

Figure 6.3. Big Bend National Park five-year light extinction budget. All days with that fall on the same day of the year were averaged together, then the data were smoothed using a 15-day moving average.

6.1.2 Apportionment of Big Bend's Sulfate Haze

Ambient particulate sulfate compounds result from direct emissions of sulfate (primary sulfate) or are produced by chemical transformation (oxidation) of SO_2 emissions in the atmosphere (secondary sulfate). Secondary sulfates constitute most of the particulate sulfate compounds measured at ambient monitoring sites, such as Big Bend National Park. The extent of the oxidation of SO_2 to secondary sulfate depends on the oxidative capacity of the atmosphere, which is influenced in large part by nitrogen oxides (NO_x) and volatile organic carbon emissions. Oxidation of SO_2 to sulfate can be slow, often requiring one to two days to convert about half of the SO_2 to particulate sulfate compounds. However, this extent of transformation can occur much more rapidly, from a few hours to several minutes, in the presence of mists, fogs, and clouds. Meanwhile, atmospheric dispersion and deposition processes are reducing the ambient SO_2 and sulfate concentrations during transport from emission sources to distant monitoring locations. Consequently, it is typically challenging to establish causal relationships between measured ambient particulate sulfate concentrations and SO_2 emissions sources.

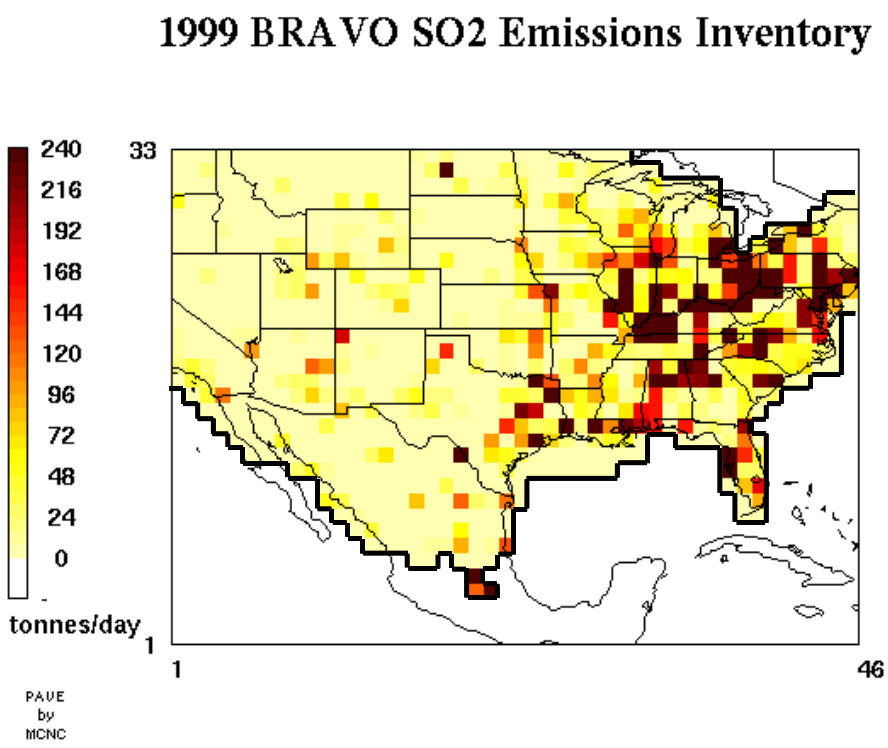

Figure 6.4. (Left) SO_2 emissions based on the 1999 BRAVO emissions inventory used in the REMSAD and CMAQ-MADRID modeling. No emissions were included beyond the black outline shown in the figure. Mexico City and Popocatepetl volcano emissions are located in the three most southern emission grid cells.

Figure 6.4 presents the SO_2 emission inventory used in the BRAVO study. As noted on the map the BRAVO study emission inventory did not include sources in southern Mexico (except for Mexico City and the Popocatepetl volcano), Cuba, or other Caribbean islands. Effects of sources outside of the modeling domain, beyond the frames of Figure 6.4, were accounted for in BRAVO study modeling by use of four-month average boundary conditions obtained from global model simulations. The largest SO_2 emissions are in the eastern United States where about 14 million tonnes/year are emitted. In Texas approximately 1 million tonnes of SO_2 are emitted each year, almost all in eastern Texas, and the western U.S. emissions are about 1.7 million tonnes/year. In Mexico, SO_2 emissions are estimated to be about 2.5 million tonnes/year, with 1.5 million tonnes/year from the Popocatepetl volcano. There are a few high-emitting locations in northern Mexico, including the Carbón I & II coal-fired power plants located about 200 km east-southeast of Big Bend and at urban and industrial areas near Monterrey in northeastern Mexico.

U.S. SO_2 emission inventories have been in development for over 30 years, and in the 1990s continuous emission monitors were placed into the largest SO_2 point sources. Therefore the U.S. SO_2 emission inventory is considered to be of a high quality. However, less information was available about the Mexican SO_2 emissions and significant uncertainties in the inventory remain. For example, a recently produced emission inventory for Mexico differs from the BRAVO emissions inventory for SO_2 emissions, with emissions by as much as a factor of two larger in some regions. In addition, uncertainties in Carbón SO_2 emissions exist and emissions of 154,000 and 245,000 tonnes/year were used.

The Popocatepetl volcano in central Mexico near Mexico City has been active for a number of years including during the BRAVO study period and is the largest single SO_2 emissions source in North America. Limited modeling of the flow of its emissions indicated that it likely had little effect on Big Bend haze during the BRAVO study period. The effects of emissions from southern Mexico, Cuba, and other areas outside of the BRAVO study emissions inventory are also thought to be small at Big Bend.

6.1.2.1. Spatial Patterns of Aerosol Components

Examination of the spatial and temporal patterns in several fine particulate species, including sulfate, measured during BRAVO suggests that there are unique sources for different aerosol types and that transport patterns are seasonal with more transport from Mexico to southern Texas during the summer than during the fall and conversely more transport from the eastern United States during the fall than during the summer. These findings are consistent with the back trajectory analyses. Sulfate concentrations at Big Bend were highest during four episodes, September 1 and 2, 14 and 15, October 12, and August 22. The four episodes were characterized by different trace element concentrations and different spatial patterns in sulfate, indicating differing contributions from different source types for each episode. Sulfate concentrations measured within a few hundred km are generally highly correlated in time, but measurements in southwestern Texas were not highly correlated with measurements in northeast Texas, and different regions of the state also had different seasonal patterns in sulfate concentrations, indicating they are influenced by different sources. Highest sulfate concentrations measured during BRAVO were in northeast Texas during the summer, while highest concentrations at Big Bend were during the fall. Spatial patterns in sulfate concentrations show influence from the Carbón I & II power plants, especially north and west of the plants, though the contribution is not quantifiable by these analyses.

Spatial and temporal patterns in the iron concentrations and the abrupt drop in Al/Ca ratios from summer to fall are evidence of Saharan dust episodes during the summer.

The trace element most associated with sulfur at Big Bend is selenium, which is usually associated with coal combustion. Selenium concentrations were highest in northeast Texas, with evidence of selenium sources within the state, at the Carbón I & II plants, and possibly entering Texas from the east.

6.1.2.2. Airmass Transport to Big Bend during BRAVO Days with High and Low Particulate Sulfate Concentrations

All other things being the same, a source region's potential to contribute to haze at Big Bend increases for time periods when air parcels frequently pass over and spend more time over the source region prior to transport to Big Bend. These airmass transport characteristics can be estimated from trajectories, where a trajectory gives the estimated location of air parcels every hour prior to their being transported to Big Bend. Residence time analysis is used to aggregate the number of air parcels that resided over an area for selected periods of time at Big Bend (e.g., a month) or selected receptor site conditions (e.g., haziest days at Big Bend). This is related to the aggregate of time all trajectories resided over a given area. While the residence time is dependent on airmass transport frequency from a given region to Big Bend and the time it spends

over the region, it has been shown that the difference in the residence time from one region to another is primarily dependent on different transport frequencies.

On days with the 20% highest particulate sulfur concentrations during the BRAVO study, air parcels were most likely to have previously resided over northern Mexico, Texas, and the eastern United States (Figure 6.5a). These tended to be low-level and low-speed air parcels, which are conducive to the accumulation of pollutants from sources. In contrast, on days with the 20% lowest particulate sulfate concentrations, air parcels were most often previously over northern Mexico and the Gulf of Mexico as well as over the western United States and infrequently over eastern Texas or the eastern United States (Figure 6.5b). The transport over Mexico tended to be low level but high speed, which is not conducive to the accumulation of emissions into the air parcels.

The examination of transport pathways during individual particulate sulfate episodes showed that there were three common pathways associated with elevated sulfate at Big Bend, from eastern Texas, the southeastern United States., and northeastern Mexico (Figure 6.6). The largest concentrations occurred when transport over several of these regions occurred. For example, the September 1 episode had transport over all three regions and had the highest concentrations during the BRAVO study. Elevated sulfate was also associated with prior transport over the Midwest (Missouri, Kentucky, and Tennessee), though this was infrequent and airmasses tended to be elevated and had higher speeds relative to the other three regions.

These results show that the transport from eastern Texas and the southeastern United States is associated with elevated sulfate concentrations at Big Bend and is not associated with low sulfate concentrations. These results, combined with the fact that eastern Texas and the Southeast have high sulfur dioxide emissions, support the notion that these areas contribute to the sulfate concentrations and haze at Big Bend. Northeastern Mexico appears to be a common transport pathway during both high and low sulfate days. However, the time airmasses spend over northern Mexico prior to reaching Big Bend is greater on the high sulfate days than the low sulfate days. The increased time allows for potentially greater accumulation of SO_2 emissions and time for transformation to sulfate.

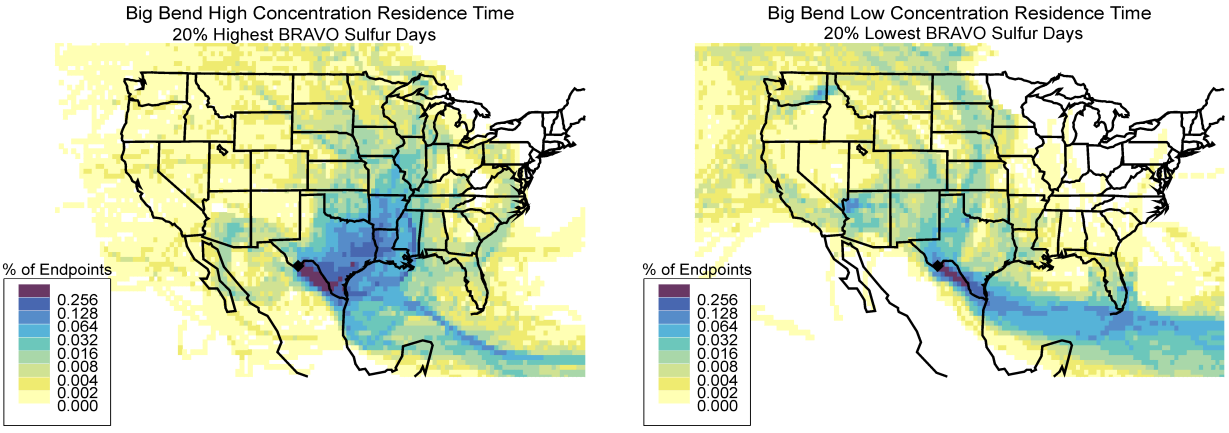

Figure 6.5. Fraction of time that air parcels spent during ten-day trajectories for periods with the a) 20% highest concentrations of particulate sulfate compounds and b) for the periods with the 20% lowest concentrations of particulate sulfate during the BRAVO study period July through October 1999.

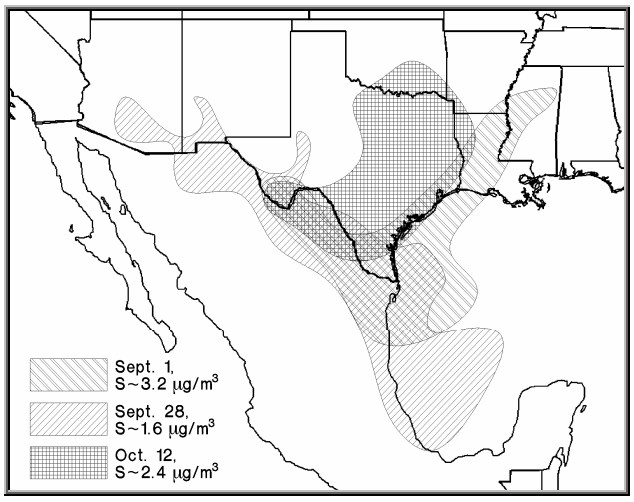

Figure 6.6. Airmass transport patterns to Big Bend, TX, during three sulfate episodes. Each isopleth shows the most likely pathway the airmass traversed prior to impacting Big Bend.

6.1.2.3. Quantitative Source Apportionment of Big Bend's Sulfate Haze

NPS/CIRA employed numerous methods to identify the source types (e.g., power plants) or source regions (e.g., Texas, the eastern United States, the western United States, and Mexico) that contribute to the particulate sulfate compounds that influence Big Bend haze and to estimate the magnitude of their contributions. The techniques fall into three categories, receptor-oriented modeling, source-oriented modeling, and hybrid modeling combining features from both source and receptor modeling.

Airmass-History-Based Receptor Models: Several airmass-history-based receptor analysis methods were used for source attribution. These methods developed statistical relationships between the Big Bend particulate sulfate concentrations and airflow prior to reaching Big Bend. Variations of the trajectory methods included the use of two methods of estimating wind over North America (EDAS from the National Weather Service and MM5 applied specifically for the BRAVO study) and the use of back-trajectories from Big Bend employed in Trajectory Mass Balance (TrMB), and forward transport and dispersion from all potential source regions used in Forward Mass Balance Regression (FMBR).

Extensive testing of TrMB and FMBR applied to both sets of wind information showed adequate overall performance when used to attribute artificial tracer released as part of the BRAVO study. Additional evaluations showed that these airmass history regression models were accurate within their stated precision when applied to synthetic sulfate concentration with known attribution results. Only the combination of airmass history model and meteorological data inputs that passed these evaluations was used for attribution of measured sulfate.

An inherent characteristic of these techniques is the estimation of the average relationship between air transport from an area and that area's contribution to sulfate. Therefore, these techniques were used only for estimating average attributions. These techniques are subjected to increased uncertainties due to collinearity of transport from multiple source regions. For example, transport from the eastern United States typically traversed Texas in route to Big Bend. In addition, other issues can bias the results. For example, it was found that FMBR tended to

enhance attributions to nearby source regions and reduce attribution from more distant source regions.

Regional Air Quality Source-Oriented Models: The REMSAD regional air quality model was used to estimate the effects of transport, dispersion, chemical transformation, and deposition on emissions, and thereby to predict particulate sulfate concentrations throughout the modeling domain, including at Big Bend. The difference in predicted concentrations between air quality model prediction with all emissions (base case) and those with emissions for a specific source or source region set to zero (emissions sensitivity case) is interpreted as the particulate sulfate attributed to the specific source or source region. The CMAQ-MADRID air quality model was also operated by EPRI and Atmospheric and Environmental Research (AER).

Eulerian air quality models are limited by the soundness of emissions and meteorological data, as well as the accuracy of transformation, deposition, dispersion, and other numerical algorithms. Biases and uncertainties identified in any of these processes can adversely affect their source attribution estimates. The Eulerian models were tested against the BRAVO tracer data to evaluate their capability of simulating dispersion in Texas where it was found that they could reproduce the tracer concentrations within the inherent uncertainty of the tracer data. Also, the simulated sulfate and SO_2 concentrations and sulfate apportionments were extensively compared to measured data. It was found that both models tended to underestimate particulate sulfate compound concentrations in the first half of the BRAVO study period when sources in Mexico were determined to have the largest contribution. Both models also tended to overestimate particulate sulfate concentrations when flow was from the eastern United States.

Hybrid Modeling - Synthesis Inversion Analysis of Air Quality Models: Concerns about possible systematic biases that could be the result of Mexico's SO_2 emissions and/or transformation chemistry biases resulted in the development of a hybrid modeling approach. This approach entailed the development of statistical relationships between the daily source attribution results from REMSAD and CMAQ-MADRID and the measured particulate sulfate concentrations in and around Big Bend.

The synthesis inversion technique was unable to resolve distant source regions with small source contributions. To minimize problems caused by this behavior, attribution results for these sources were held close to their originally modeled values. Thus, any sulfate that may have been improperly attributed to small distant sources by the Eulerian models runs was most likely attributed to source regions near Big Bend in the synthesized method. The technique also systematically underestimated the measured sulfate data. It is not known if this underestimation impacts one source region more than another.

It was determined that Synthesized CMAQ-MADRID combined with the attribution of Carbón power plants from Synthesized REMSAD provided the best available estimates of the source attribution for particulate sulfate at Big Bend during the BRAVO study period, henceforth referred to as the BRAVO Estimate.

Figure 6.7 shows the study period-averaged attribution results for nine methods as well as the BRAVO Estimate results. CMAQ-MADRID and Synthesized CMAQ-MADRID attribution did not include the Carbón power plants. TAGIT was a source attribution technique employed

by the Desert Research Institute (DRI) to attribute Carbón power plants' contribution to Big Bend's sulfate.

As shown in Figure 6.7, during the BRAVO study period U.S. sources contributed to about 55% (BRAVO Estimate) of the particulate sulfate at Big Bend, with a range among methods of 44% to 67%. The Mexico sources contributed about 38% of Big Bend's particulate sulfate, with a range among methods of 23% to 55%. The eastern United States was the largest U.S. contributor at ~30%, followed by Texas at ~17%, and the western United States at ~9%, with ranges among the methods of 16% to 42%, 16% to 30%, and 0% to 14%, respectively. The Carbón power plants in Mexico contributed to about 20% of the particulate sulfate at Big Bend, more than any other single SO_2 emissions facility, with a range among the methods of 14% to 26%.

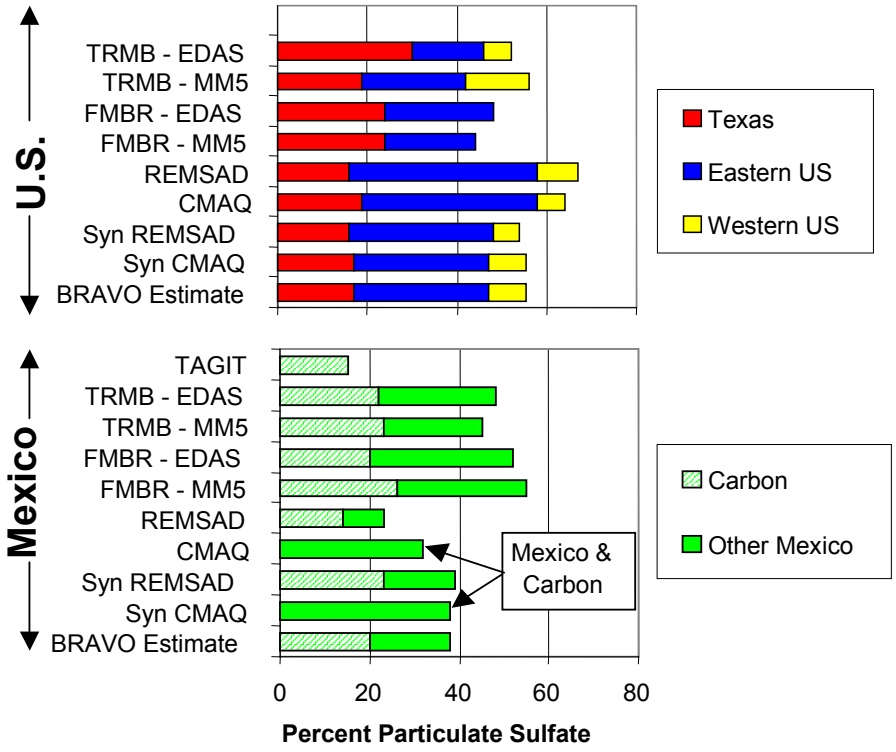

Figure 6.7. Estimates by several data analysis and modeling methods of the study-period averaged percent contributions to particulate sulfate at Big Bend by U.S. and Mexico sources. TAGIT only attributed the Carbón power plants, while CMAQ and Synthesized CMAQ attribution did not distinguish Carbón from Mexico.

Figure 6.8 presents a smoothed daily attribution using the BRAVO Estimate method. The top plot in Figure 6.8 shows attribution in absolute concentrations for direct comparison to the measured particulate sulfate concentrations, while the bottom plot shows the percent fraction of the predicted amount by each source region. As shown, each source region's contribution to Big Bend particulate sulfate had unique characteristics over the BRAVO study period. Sources in Mexico were the largest contributors to sulfate in July and August, contributing from 0.5 to 1.5 $\mu g/m^3$ every day. During the largest peak in late July, sources in Mexico contributed to about 2 $\mu g/m^3$, constituting about 90% of the modeled particulate sulfate. In September and October

contributions by sources in Mexico decreased to roughly less than 1 μg/m^3. Sources in Texas contributed very little to sulfate concentrations in July, with three episodes in the middle months of the study period having peak values from about 0.8 to 1.5 μg/m^3. During two episodes in October, sources in Texas had peak contributions of about 1.2 to 2.8 μg/m^3 of particulate sulfate and constituted to over 60% of the largest peak in October. Sources in the eastern United States contributed to sulfate concentrations mostly in the middle two months of the study period with several peak contributions exceeding 1 μg/m^3. The largest of these contributions is greater than 5 μg/m^3 and constitutes about 80% of the largest peak particulate sulfate measured during the BRAVO study period.

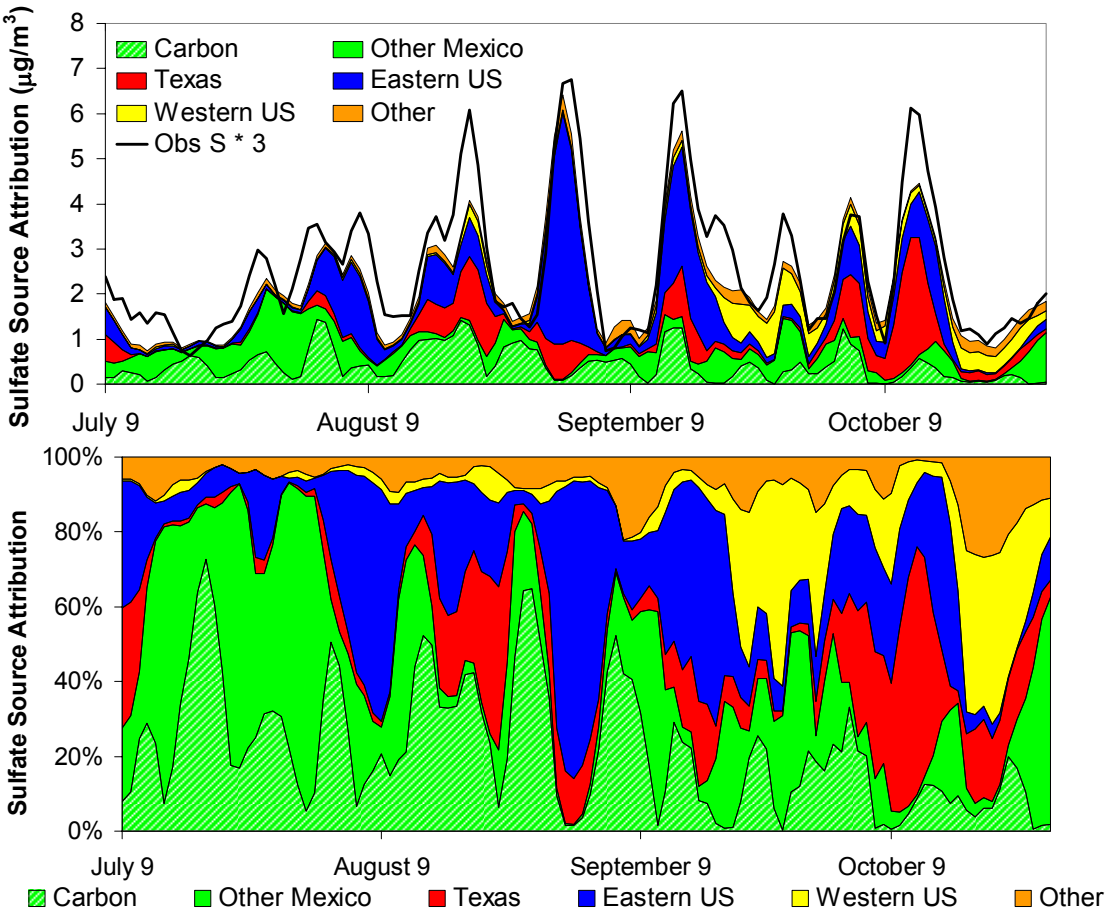

Figure 6.8. Smoothed daily estimates by source regions to particulate sulfate concentration (top plot) and fraction of total predicted particulate sulfate (bottom plot) at Big Bend during the study period.

6.1.2.4. The Contribution of Sulfur Source Regions to Particulate Haze Levels at Big Bend National Park during the BRAVO Study Period

Both the fraction of light extinction associated with particulate sulfate (see Figure 6.2) and the fraction of particulate sulfate attributed to each source region (see Figure 6.8) varied considerably throughout the BRAVO study period. This information was combined to show variation in the absolute and percent fractional contribution by sulfur source regions to Big Bend light extinction (shown in the top and bottom plots of Figure 6.9, respectively). Pie diagrams are shown in Figure 6.10 to illustrate the differences in particulate sulfate contributions by various

source regions to light extinction for the study period's 20% haziest days compared to the study period's 20% least hazy days. The numbers of 20% haziest days during each month of the BRAVO study from July through October are 1, 8, 10, and 4, respectively, while the numbers per month for the 20% least hazy days were 3, 1, 10, and 9, respectively.

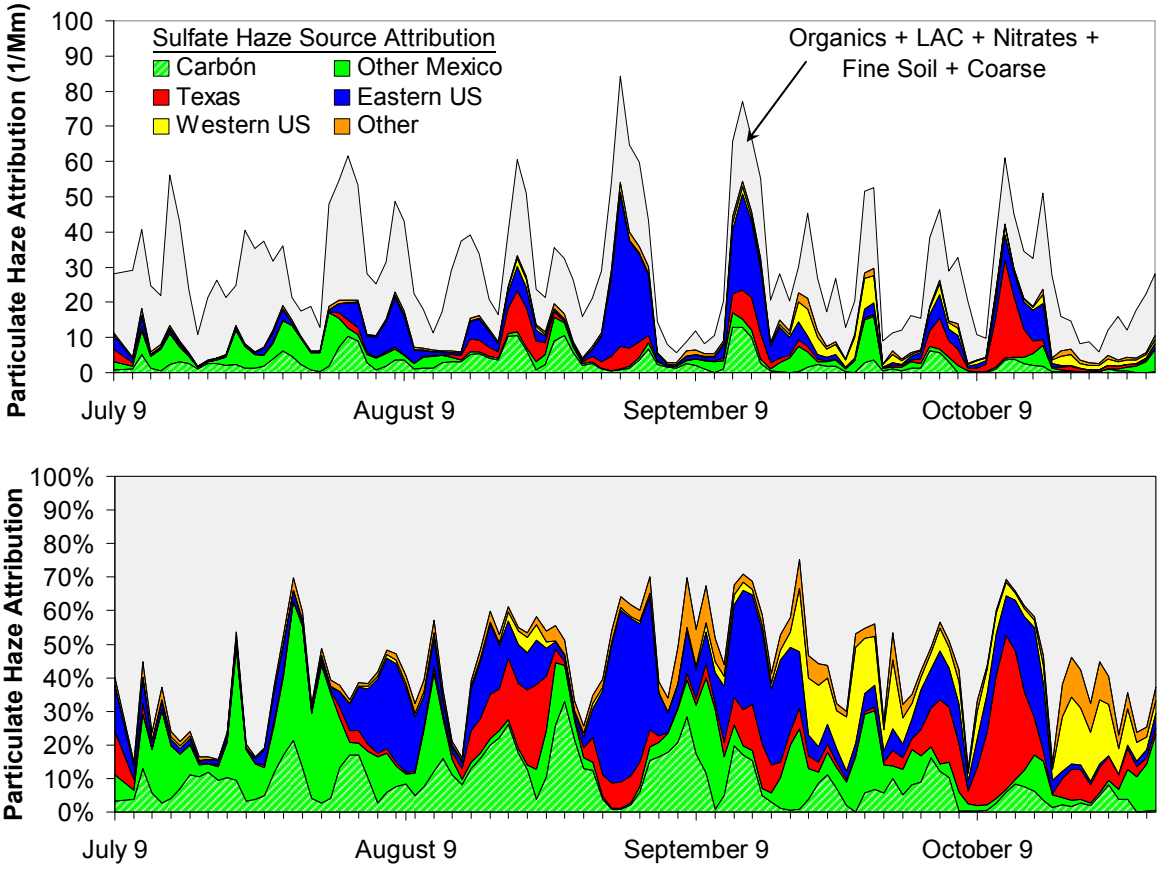

Figure 6.9. Estimated contributions to particulate haze by various particulate sulfate source regions. The top plot shows the absolute haze contributions by the various particulate sulfate sources as well as the total particulate haze level (black line). The bottom plot shows the fractional contribution to haze by the various sources.

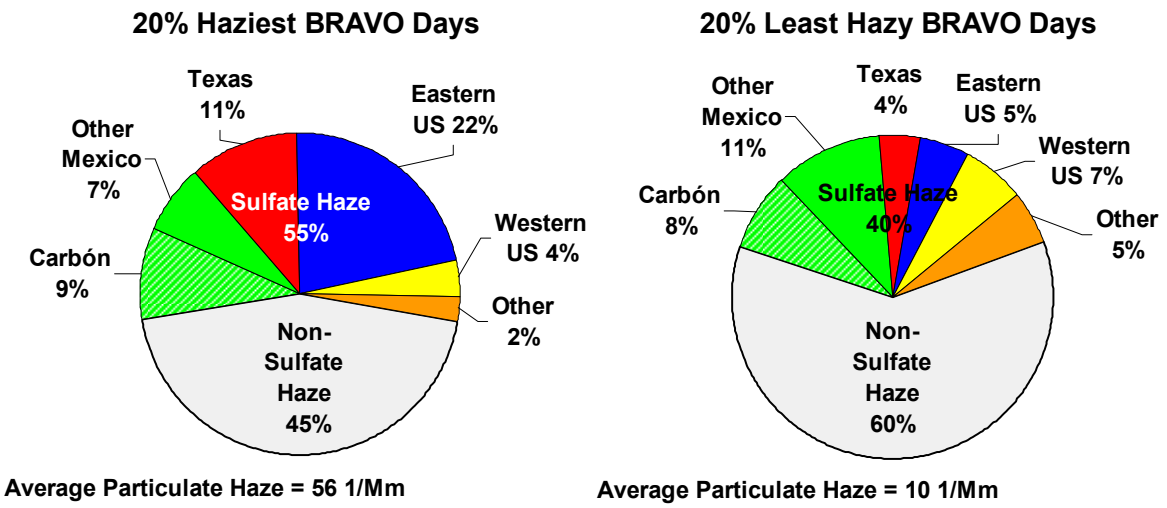

Figure 6.10. Estimated contributions by particulate sulfate source regions to Big Bend particulate haze levels for the 20% haziest days and the 20% least hazy days of the BRAVO study period.

The SO_2 sources in Mexico generally contributed a moderate 5 Mm^{-1} to 15 Mm^{-1} of the light extinction on most days during the study period, but during some of the minor haze episodes in July and August their relative contributions were 40% to 60% of the average particulate light extinction. SO_2 sources in Texas contributed to less than 5 Mm^{-1} on most days during the study period, but during one of the few periods of higher contribution these sources contributed to nearly 30 Mm^{-1}, corresponding to about 50% of the particulate light extinction on the haziest day in October. SO_2 sources in the eastern United States also contributed to less than 5 Mm^{-1} on most days during the study period, but during the two haziest episodes of the study period these sources contributed to about 50 Mm^{-1} and about 30 Mm^{-1}, respectively, corresponding to about 50% and 30% of the light extinction.

The sulfate contribution to particulate light extinction is higher on the haziest days compared to the least hazy days (55% compared to 40%). This increase in the sulfate contribution on the haziest days compared to the least hazy days is driven by increased relative contributions from the eastern United States and Texas. The relative contribution of sulfate on the haziest days from Texas increased by about a factor of 3 (4% to 11%), and from the eastern United States it increased by about a factor of 4 (5% to 22%) compared to the least hazy days. In contrast, the relative contributions for the Carbón I & II power plants remained about the same at 8% to 9%, and the contribution of other sources in Mexico decreased from 11% on the least hazy days to 7% on the haziest days. The relative contribution of sulfate sources in the western United States to Big Bend's sulfate haze also decreased from 7% on the least hazy days to 4% on the haziest days. These results are consistent with the observation that the Texas and eastern U.S. sources had their largest sulfate contributions during the highest sulfate episodes.

The nonsulfate haze is primarily due to dust (fine soil and coarse particles) and carbonaceous (organic and carbon) compounds. Compared to the least hazy days, the haziest days have a higher relative contribution to light extinction by dust (25% compared to 19%) and a lower relative contribution by carbonaceous particles (19% compared to 39%).

6.1.3 Application of the Source Attribution Results to Other Months and Years

In order to assess the applicability of haze attribution results for the BRAVO study to other years or other times of year, it is necessary to compare the four-month study period with the same months in other years and with other months of the year. Emissions and meteorology are the two most important factors that influence haze levels. Between 1999 and the present, the annual emissions responsible for particulate sulfate concentrations in North America have not appreciably changed (U.S. emissions have decreased about 15%, but less is known about emission trends in Mexico). Seasonal variations in SO_2 emissions and in the SO_2 to particulate sulfate oxidation rate make extrapolations of the BRAVO study results to other months of the year prone to additional uncertainty. One of the most influential meteorological processes affecting the haze at Big Bend is the airflow patterns that determine which potential source regions are upwind of Big Bend. In spite of the uncertainties inherent in such a simple approach, comparisons of the meteorological flow patterns from the residence time analysis were used alone in an attempt to assess the applicability of BRAVO study results to other years and times of year.

Residence time plots convey information about both the frequency of transport over potential source regions and its duration over the regions. However, it was shown that the residence time transport patterns are primarily driven by the variations in transport frequency over regions as opposed to duration variations. Consequently, a change that doubles the residence time over a source region for a specific month can be thought of as doubling the probability of influence of that source region during that month. In this example the monthly averaged contribution would likely double because the numbers of impacting periods would about double, but the amount of the peak impact is not expected to change much.

During the BRAVO study period, airflow to Big Bend was mostly similar to the airflow conditions during the five-year period. However, in September 1999 there was typically less flow over the eastern United States than for the five-year average, implying that the BRAVO results may underestimate the average haze contributions by that region's sources. In addition, during October 1999 there was typically more flow over Texas and less flow over Mexico, implying that the average October BRAVO haze contributions may be overestimated for Texas and underestimated for Mexico compared to the five-year average. While the estimated average contributions by these source regions may change, the peak contributions are likely not affected by the atypical frequency of flow.

Comparing the airflow patterns for the BRAVO study period to that of the other months of the year (Figure 6.11), it is evident that SO_2 sources in Mexico are likely to contribute less from November through March. This is because airflow across Mexico is less in general and is over lower emission density regions of Mexico to the west of Big Bend. SO_2 sources in Mexico are likely to be contributing to the particulate sulfate portion of the Big Bend haze during the months of April through June comparable to their contributions for the BRAVO study months of July and August. Sources in Texas are likely to contribute little to the particulate sulfate portion of the Big Bend haze for the months from November through June since the airflow is not frequently over the high emissions regions of east Texas, similar to July 1999. Eastern U.S. sources are unlikely to contribute to Big Bend haze during the months from November through March since airflow to Big Bend is rarely over that region during those months. During the

months from April to June, the eastern U.S. sources may contribute a modest amount to sulfate haze, comparable to that estimated for July and early August.

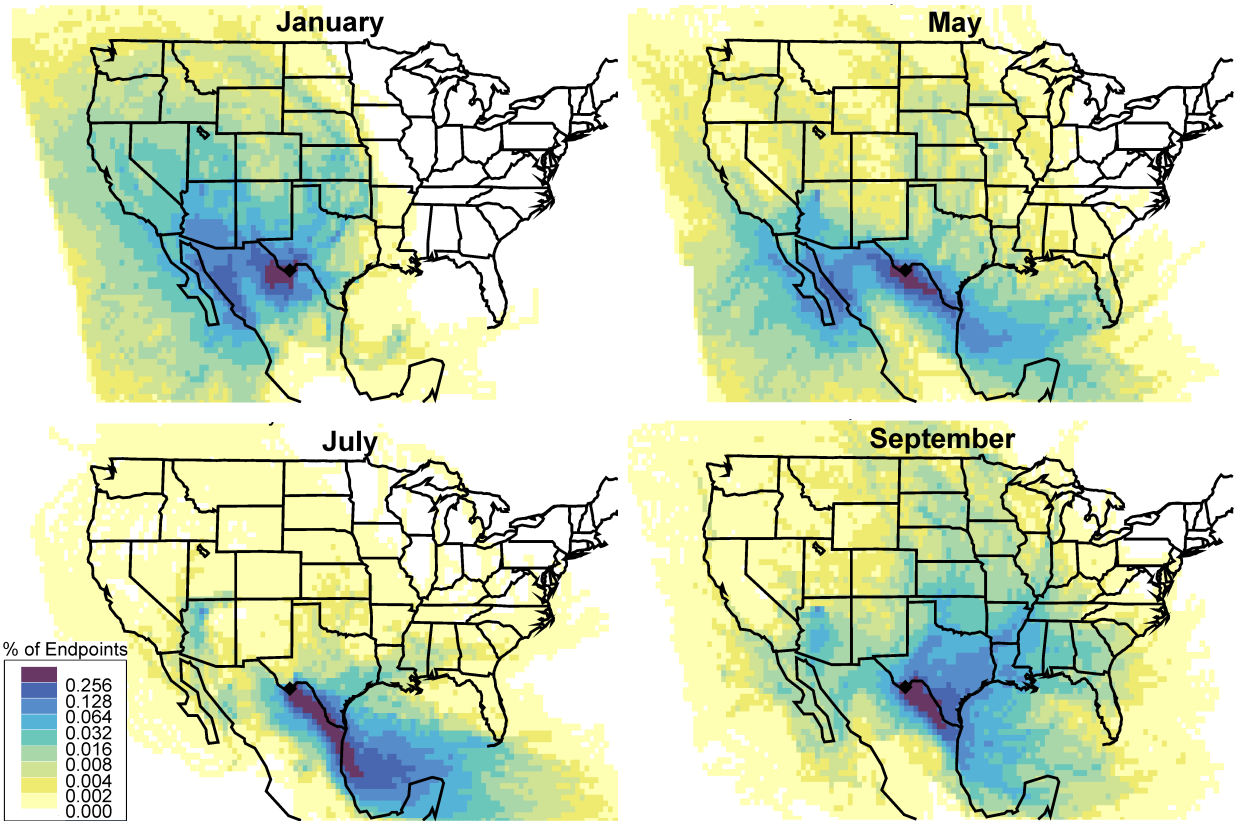

Figure 6.11. Examples of geographic distribution of the fraction of time that air parcels spend during the five days prior to arriving at Big Bend National Park for the months of January, May, July, and September based upon a five-year analysis period (1998 to 2002).

6.1.4 Implications

There is no single answer to the question of what sources are responsible for the haze at Big Bend National Park; sources in both the United States and Mexico are responsible. Mexican SO_2 emissions contribute to the sulfate haze most frequently, but to generate the haziest events that occur in the late summer and fall, contributions from Texas and the eastern United States must occur. The greatest individual contributor to haze is the Carbón I & II power plant in northern Mexico. Substantial changes of that facility's emissions would likely result in small but noticeable changes in haze levels on many days, but it would not make much difference to the worst haze episodes during late summer and early fall. To substantially affect all of the haze episodes during the late summer and fall where U.S. contributions are large at Big Bend will require SO_2 emission changes in both Texas and the eastern United States. Because of the high frequency of air transported to Big Bend from the southeast along a corridor on both sides of the Rio Grande River, emission changes there have a potential to affect haze levels at Big Bend, especially during June through September when transport from this region is most frequent.

The clearest days at Big Bend also had low sulfate concentrations. The visual scene on a clear day is more sensitive to small changes in haze than a hazy or moderately hazy day. These

days were primarily associated with contributions from the Carbón I & II power plants and other sources in northeast Mexico. Reduction in emissions from Carbón would likely result in creating more clear days. On the other hand, growth along this border region will likely further reduce the number of clear days.

6.2 EXECUTIVE SUMMARY: THE YOSEMITE AEROSOL CHARACTERIZATION STUDY

The Yosemite Aerosol Characterization Study (YACS) was an intensive field measurement campaign conducted by a number of U.S. research groups from 15 July to 4 September 2002 at Yosemite National Park (NP), California. This summary describes the major findings of the study in the context of outstanding issues related to the Regional Haze Rule and to visibility and air quality concerns specific to Yosemite NP.

Aerosol composition measurements have been conducted in Yosemite NP since 1988 as part of the Interagency Monitoring of Protected Environments (IMPROVE) network. The long-term data record (1988–2004) clearly shows a seasonal trend in organic aerosol mass concentrations, with peaks in the summer and early fall (Figure 6.12). The long-term Yosemite data show that organic carbon contributes between 40 and 60% of the monthly average fine aerosol mass. These fractions are much higher than most IMPROVE sites in the eastern United States. Not only the total fine particulate mass concentration, but also the fraction attributable to organic species, increases during summer and fall. Furthermore, the variability in organic aerosol mass concentrations becomes much larger in those seasons.

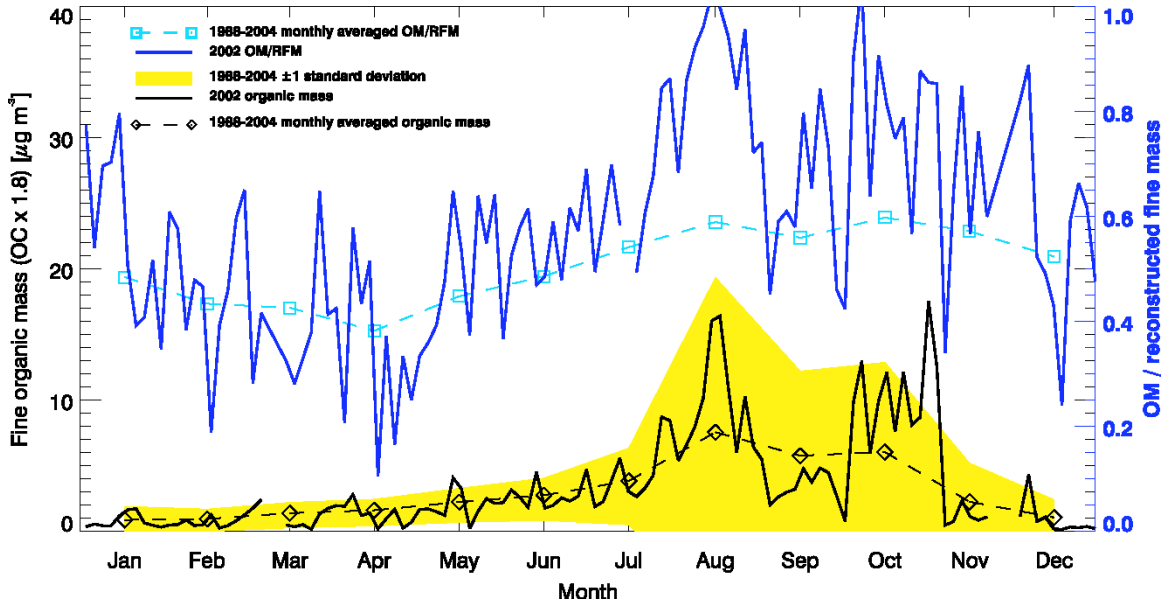

Figure 6.12. Annual variation of organic carbon mass concentrations in the fine mode of the aerosol ($PM_{2.5}$), from data obtained from the IMPROVE database (http://vista.cira.colostate.edu/views/). A measure of interannual variability is indicated by the yellow shaded area, which envelops one standard deviation in the data. Blue lines indicate the fraction of fine particulate mass concentration apportioned to organic carbon over the long-term average and for 2002.

These observations suggest an important role for organic carbon in air quality and visibility degradation in Yosemite NP. However, at the time this study was planned, several key properties of aerosol organic carbon were unknown, all of which affect estimates of visibility impairment.

- First, organic carbon in atmospheric aerosols exists in molecular forms that incorporate hydrogen, oxygen, nitrogen, and possibly other elements. However, the standard IMPROVE analytical technique measures only carbon concentrations, and thus a multiplication factor that accounts for additional weight contributed by other elements is needed to determine the total organic aerosol mass concentration in the atmosphere. Although a factor of 1.4 is used for this conversion in the Regional Haze Rule, recent studies suggested this factor may not be appropriate for many of the rural and remote locations represented in IMPROVE. The study design included measurements that could be used to constrain total mass and thus to deduce appropriate conversion factors for summertime Yosemite aerosols.
- Second, it was unknown whether the organic carbon fraction of the total aerosol could absorb water in response to increases in ambient relative humidity; standard IMPROVE and Regional Haze Rule visibility calculations assume it cannot. The absorption of water can dramatically increase total atmospheric aerosol mass concentrations and also tends to enhance extinction per unit mass. Both effects can significantly increase estimates of visibility impairment and thus need to be accurately modeled. To address these questions, the study design included measurements to quantify the increase in extinction, as a function of relative humidity, due to water uptake by aerosol organic carbon.
- Finally, the standard IMPROVE measurements can provide little insight into the sources of aerosol organic particulate matter, although the increased variability and occurrence of higher organic aerosol mass concentrations during years having severe wildfire seasons suggest that wildfire emissions are important. However, tourism in Yosemite NP follows a similar seasonal trend. Elucidation of the respective contributions of wildfire emissions and transportation sources to particulate organic matter concentrations in Yosemite NP was a third key objective of the Yosemite Aerosol Characterization Study. Sampling occurred at the elevated Turtleback Dome site, the location of the long-term IMPROVE monitors, and at a ground-level site in Yosemite Valley.

6.2.1 Study Objectives

- Determine appropriate values for converting analyzed aerosol carbon mass to ambient aerosol organic carbon mass.
- Develop an improved understanding of the visibility-impairment-related characteristics of a smoke/organic carbon-dominated aerosol, including the role of relative humidity in modifying visibility impairment.
- Examine the sources contributing to high aerosol organic carbon mass concentrations.

6.2.2 Study Findings

- **Accurate modeling of the effects of aerosols on summertime visibility in Yosemite NP requires revision of several commonly applied assumptions.**
  - The total mass of organic compounds present in fine particulate matter at Turtleback Dome was better represented by multiplying elemental carbon concentrations by 1.8, rather than by 1.4 (Figure 6.13). The commonly applied 1.4 factor underestimated the total mass concentration of fine-mode organic aerosol by more than 25%. This higher

multiplier suggests that a significant fraction of the aerosol organic matter comprised highly oxygenated organic species.

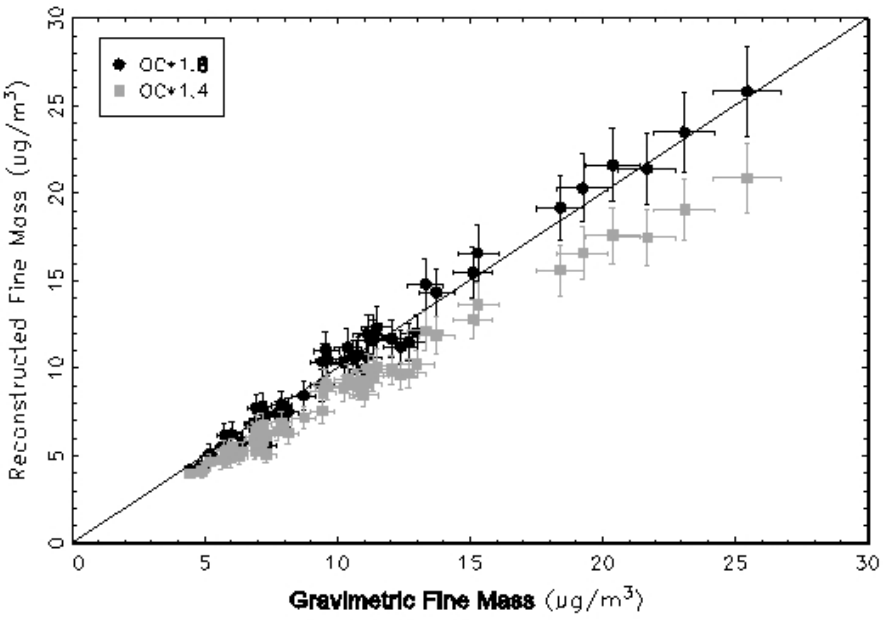

Figure 6.13. Fine mass concentrations reconstructed from individual species concentration measurements, plotted against fine mass concentrations determined by gravimetry (weighing of filters). Reconstructions are shown for two assumptions regarding the elemental-to-molecular mass conversion for organic carbon.

- The average dry mass scattering efficiency of the $PM_{2.5}$ aerosol was determined to be close to 4 m^2 g^{-1}, the same value used in the IMPROVE protocols to estimate dry light scattering coefficients of organic carbon particulate matter. However, during periods of high fine mass concentrations dominated by organic carbon and influenced by fire emissions, the dry mass scattering efficiencies ranged as high as 6 m^2 g^{-1}. The standard IMPROVE formula thus underestimates the contribution of organic carbon to total light scattering by as much as 50% during these periods.
- Light absorption was better modeled if it was assumed that elemental carbon was mixed with other constituents in individual particles, rather than assuming it was present as a separate mode. Single-particle analyses by electron microscopy also suggested that aerosol constituents were mostly found together in individual particles. IMPROVE formulas base the optical properties of elemental carbon on the assumption that it is not mixed with other aerosol species.
- At 85% relative humidity, aerosol light scattering coefficients are enhanced by a factor of 1.1 to 1.3 due to the presence of condensed water in the aerosol phase. This is much lower than the factors expected for aerosols dominated by sulfate compounds.
- Nitrate in the fine particle mode was associated most often with reacted sea salt and was only occasionally present as ammonium nitrate, which is the assumed molecular form in IMPROVE conversion equations. The reacted sea salt is present primarily in the coarse mode, although some of this mass is captured and detected on the $PM_{2.5}$ filter samples. Nitrate associated with coarse sea salt particles has a lower impact on visibility per unit

mass than is assumed for fine mode ammonium nitrate in the IMPROVE equations. However, this is partially compensated for by lower estimates of nitrate species mass concentrations, because the molecular mass of sodium nitrate is slightly larger than that for ammonium nitrate.

- **Organic carbon was the dominant component of fine particulate matter in Yosemite NP during summer 2002, and $PM_{2.5}$ mass concentrations were higher than long-term average concentrations.**
  - Figure 6.14 shows the study-averaged fine ($PM_{2.5}$) aerosol composition as observed at Turtleback Dome and at the Yosemite Valley site, along with an estimate of the coarse mass concentration (PM_{10}-$PM_{2.5}$). Organic carbon represented, on average, more than 70% of the fine mass concentration at both sites.
  - The average $PM_{2.5}$ mass concentration in Yosemite Valley during the study was 16 ± 5 µg m^{-3}, and at Turtleback Dome it was 10 ± 4 µg m^{-3}. This compares with July–August average values over 1988–2004, calculated from data in the IMPROVE database for the Yosemite NP site at Turtleback Dome, of 8 ± 5 µg m^{-3}. As can be seen in Figure 6.14, most of the difference in the fine aerosol mass concentrations between the two sites was due to higher concentrations of aerosol organic carbon at the Valley Floor site.

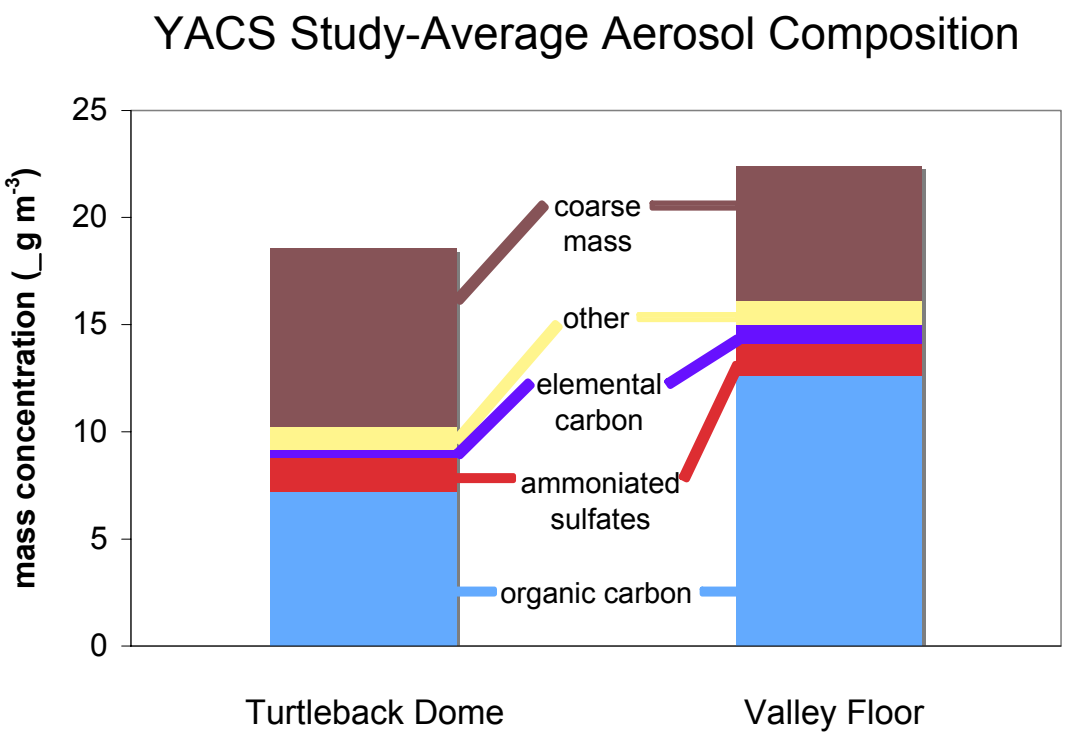

Figure 6.14. PM_{10} aerosol mass concentrations reconstructed from individual species concentration measurements, for the Turtleback Dome and Valley Floor sites.

- **Fine particles were the dominant contributor to visibility degradation at Turtleback Dome during summer 2002.**

- The average total (gas plus aerosol) extinction coefficient at Turtleback Dome was 57 ± 31 Mm^{-1}, representing the mean value ± one standard deviation. This corresponds to a visual range of approximately 69 km. The highest values of the extinction coefficient occurred in mid-August and were on the order of 191 Mm^{-1} (20-km visual range). This compares with the proposed annual average extinction coefficient for "natural background" conditions in the nonurban western United States of 15.8 Mm^{-1}.
- On average, 77% of the total light extinction coefficient was attributed to scattering by fine particles; absorption by fine particles and scattering by coarse mode particles contributed 8% and 15%, respectively (Figure 6.15).

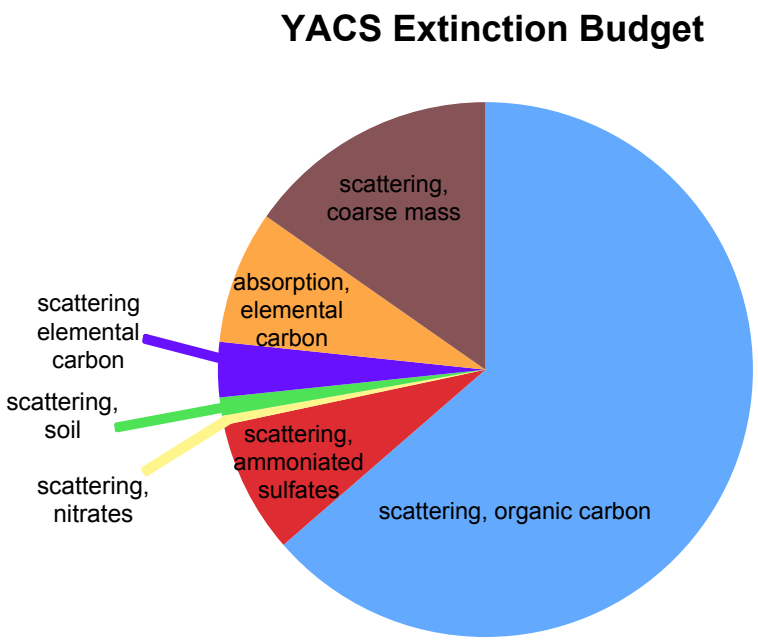

Figure 6.15. Reconstructed, study-averaged extinction budget at Turtleback Dome. All species except coarse mass are in the fine aerosol mode.

- **Natural (biogenic) sources dominated the total, and the variability in, particulate organic mass concentrations in summer 2002 at Turtleback Dome.**
  - Carbon isotope analyses of fine aerosol filter samples from Turtleback Dome determined a constant contribution from fossil fuel sources of 0.7 ± 0.1 µg m^{-3} to particulate organic matter. Contemporary (biogenically derived) carbon represented 2–9 µg m^{-3}. Sources of contemporary aerosol carbon include emissions from fires and vegetative emissions of reactive gases that subsequently form condensable species, both particulate primary emissions and volatile organic aerosol precursors that are later oxidized to secondary organic aerosols.
- **There is evidence that particulate matter sampled at Turtleback Dome was strongly influenced by the long-range transport of emissions from wildfires.**
  - During the summer of 2002, wildfires burned more than 7 million acres in the United States. Several of the largest and longest-lived fires were in southern Oregon and

California. Back and forward trajectories indicate that fire emissions were transported into California, and that a regional haze affected much of the state during August. Figure 6.16 shows an example satellite image from MODIS (http://modis.gsfc.nasa.gov/gallery/).

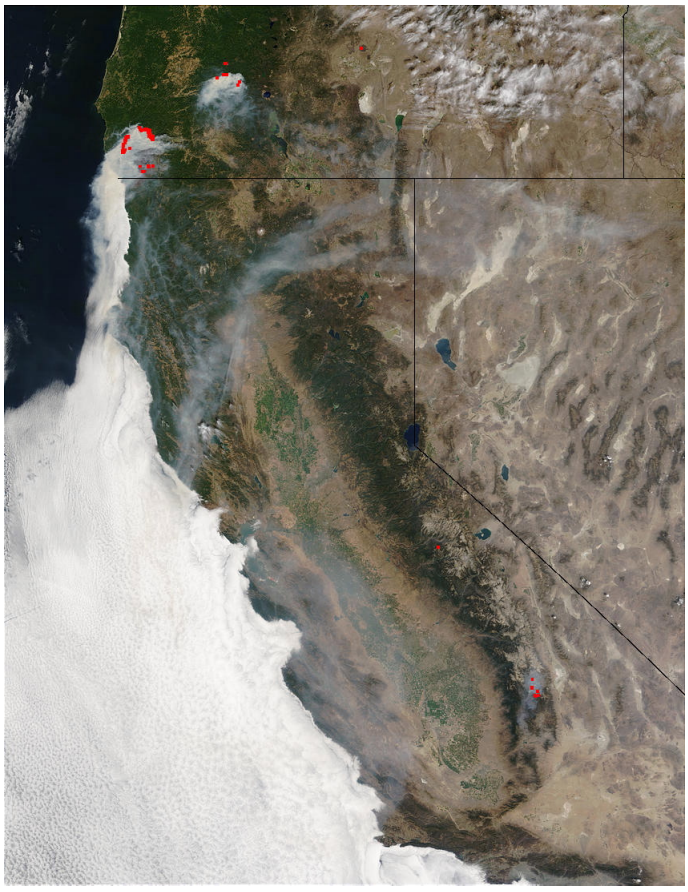

Figure 6.16. MODIS image (August 18) of smoke from fires (red areas) in Oregon and in Sequoia National Park transported into California's Central Valley.

- Back trajectory analyses and molecular marker techniques also confirmed the influence of smoke on aerosols sampled at the site. Figure 6.17 shows the study-average apportionment of $PM_{2.5}$ organic carbon measured at Turtleback Dome to various sources for which molecular markers and source signature profiles exist. The apportionment was highly variable in time, with primary wood smoke particles estimated to contribute <1% during the first week of the study to a high of 65% during the last week. Transportation sources contributed 4–19% on a weekly basis, and 10% on average, at this site. Most of the organic carbon mass could not be attributed to primary emissions from known sources and was thus assumed to be secondary in nature. Given the modern carbon signature observed in Turtleback Dome aerosol, most of the secondary material probably was derived from oxidation of biogenic volatile organic compound (VOC) emissions. VOCs associated with wildfire smoke appeared to be significant contributors to secondary organic aerosol.
- Although fewer measurements of organic aerosol speciation were available at the Valley

Floor site, data available from that location suggest a somewhat larger contribution of transportation sources to observed organic carbon.

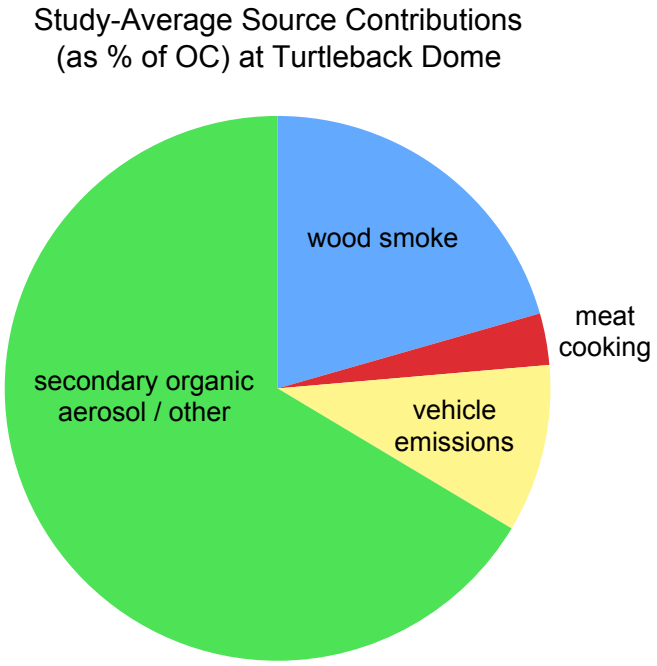

Figure 6.17. Study-averaged source contributions of fine aerosol organic carbon (expressed as % of OC) at Turtleback Dome.

6.3 EXECUTIVE SUMMARY: REVIEW OF THE IMPROVE EQUATION FOR ESTIMATING AMBIENT LIGHT EXTINCTION COEFFICIENTS

6.3.1 Introduction

Compliance under the Regional Haze Rule is based on Interagency Monitoring of Protected Visual Environments (IMPROVE) protocols for reconstructing aerosol $PM_{2.5}$ mass concentrations and light extinction coefficients (b_{ext}) from speciated mass concentrations. Dry $PM_{2.5}$ fine mass is computed using equations 1 and 2:

$$PM_{2.5} = (NH_4)_2SO_4+NH_4NO_3+POM+LAC+Soil \quad (1)$$

$$Soil = 2.2Al+2.49Si+1.94Ti+1.63Ca+2.42Fe \quad (2)$$

where sulfate is assumed to be fully neutralized ammonium sulfate ($(NH_4)_2SO_4$), nitrate is assumed to be in the form of ammonium nitrate (NH_4NO_3), and organic carbon is included as particulate organic material ($POM=R_{oc}\cdot OC$), computed by multiplying organic carbon (OC) concentrations by a molecular weight per carbon weight ratio (R_{oc}). Light-absorbing carbon is referred to as LAC. Fine soil concentrations include the contributions from assumed forms of elemental species (equation 2) (Malm et al., 1994). Mass concentrations are given in units of μg m^{-3}.

The current IMPROVE equation used to estimate total light extinction coefficients for visible wavelengths (λ) associated with measured aerosol species is

$$b_{ext}=(3.0)f(RH)[(NH_4)_2SO_4]+(3.0)f(RH)[NH_4NO_3]+(4.0)[POM]+(1.0)[Soil]+(0.6)[CM]+(10.0)[LAC] \quad (3)$$

where the nominal dry mass scattering and absorption efficiencies are in units of m^2 g^{-1} and b_{ext} is in units of inverse length. The forms of aerosol species are the same as in the reconstructed mass equations (equations 1 and 2). A value of R_{oc}=1.4 is used to compute POM. Coarse mass (CM) is computed as the difference between PM_{10} and $PM_{2.5}$ gravimetric mass ($CM=PM_{10}-PM_{2.5}$). The $f(RH)$ scattering enhancement curve accounts for the effects of relative humidity (RH) on particle growth and scattering for hygroscopic particles. Currently, it is computed assuming continuous particle growth starting at 40% relative humidity for fully neutralized pure ammonium sulfate. Only sulfates and nitrates are assumed to be hygroscopic.

Equation 3 reflects only the contribution of particulates to b_{ext}. Gaseous scattering and absorption can also be important under certain conditions. Scattering of light by air molecules is referred to as Rayleigh scattering (b_{ray}) and currently is assumed to be a constant 10 Mm^{-1} for all the IMPROVE sites, although it varies as a function of pressure and temperature. Absorption by NO_2 in visible wavelengths can also be important and is currently not included in the IMPROVE protocol.

The formulation of the equations used in the mass and IMPROVE b_{ext} reconstructions (equations 1–3) requires a number of assumptions. Each assumption has associated uncertainties with obvious consequences for reconstructed extinction, albeit to varying degrees. Uncertainty in estimated extinction is dependent on not only the assumed forms of each of the aerosol species and their respective mass scattering efficiencies and growth factors but also on measurement and

analytic accuracy and precision. We have recently reviewed the assumptions and some associated uncertainties inherent to this formulation (Hand and Malm, 2005). We suggest refinements when data exist to support modifications to the assumptions used to derive the IMPROVE equation. However, refinements of several of the assumptions are not possible at this time because existing data do not warrant them, or because further measurements are required. The suggested refinements of the IMPROVE equation include

- changing the R_{oc} factor used to compute particulate organic matter from 1.4 to 1.8
- modifying the *f(RH)* scattering enhancement curve to reflect some water associated with particles below a relative humidity of 40%
- including sea salt in reconstructed mass and extinction equations
- modifying values of dry mass scattering efficiencies to reflect current data and functional relationships between mass scattering efficiency and mass concentration
- site-specific Rayleigh scattering based on elevation and the annual average temperature of a monitoring site
- the addition of a NO_2 light absorption term used at sites with available data

The following discussion provides a brief description of the motivation behind these refinements.

6.3.2 Particulate Organic Matter and the R_{oc} Multiplier

Estimating the contributions of organic carbon aerosol to mass or scattering requires an estimate of the total mass associated with organic carbon. The organic carbon multiplier (R_{oc}) used to compute particulate organic material ($POM = R_{oc} \cdot OC$) is an estimate of the average molecular weight per carbon weight for organic carbon aerosol and takes into account contributions from other elements associated with the organic matter, such as N, O, and H. It is impossible to determine which and how many elements are associated with *POM* without knowing the chemical formula of the organic compound, and it is common for ~ 20–40% of organic aerosol mass to remain unidentified (Turpin and Lim, 2001).

Because the organic compounds that compose *POM* are largely unknown, the approach for taking into account other elements in *POM* mass has been to apply an average multiplier. The current value of 1.4 applied in the IMPROVE equation dates back to samples collected in Pasadena CA in the early 1970s and 1980s (Grosjean and Friedlander, 1975; White and Roberts, 1977; Van Vaeck and Van Cauwenberghe, 1978; Countess et al., 1980; Japar et al., 1984). More recently, Turpin and Lim (2001) reviewed estimates of R_{oc} in terms of the types of compounds known to compose *POM*. They recommend a factor of 1.6 ± 0.2 for urban organic aerosols, a factor of 2.1 ± 0.2 for nonurban organic aerosols, and values ranging from 2.2 to 2.6 for samples with impacts from biomass burning. El-Zanan et al. (2005) used solvent extractions from archived IMPROVE filters at five sites to directly measure *POM* mass and carbon content and derive an average R_{oc} of 1.92 (range of 1.58–2.58). Malm et al. (2005a) recently found that an R_{oc} factor of approximately 1.8 allowed for closure in fine mass and light scattering coefficients for periods that encompassed both pristine conditions as well as the impacts of biomass burning

and regional haze in Yosemite National Park. Poirot and Husar (2004) found better agreement between measured and reconstructed fine mass by applying an R_{oc} factor of 1.8 during a biomass burning event in the New England and mid-Atlantic state regions.

Malm and Hand (2006) estimated R_{oc} from IMPROVE data by applying an ordinary least square (OLS) multiple-linear regression (MLR) analysis using

$$PM_{2.5,i} = a_1[(NH_4)_2SO_4]_i + a_2[NH_4NO_3]_i + a_3[OC]_i + a_4[LAC]_i + a_5[soil]_i + a_6[sea\ salt]_i \quad (4)$$

where the aerosol species are the same chemical form as in equations 1 and 2, and *i* refers to a single sample (or time period). This type of analysis has inherent uncertainties, as discussed by Andrews et al. (2000) and El Zanan et al. (2005). If the mass for each species (other than *POM*) is accurately estimated and the regression is unbiased, then the regression coefficient (a_i) for a given species should equal 1. The regression coefficient for *POM* corresponds to the R_{oc} factor.

The annual mean value of R_{oc} derived from equation 4 is shown for all IMPROVE sites in Figure 6.18, with obvious spatial trends. The highest coefficients of 1.8–2.0 are just east of the Rocky Mountain range and may be reflective of wild and prescribed fire activity to the west of this region. Three of the four sites in Alaska (not shown) also have coefficients near 1.9, with the exception of Simeonof National Wildlife Refuge on the Alaskan peninsula. Other remote locations have R_{oc} values near 1.8. Coefficients ranging from 1.6 to 1.8 are found around most of the United States, with distinct regions having coefficients less than 1.6. Regions in the Northwest, interior Midwest, and Northeast are in this category.

The annual mean coefficient over all sites is R_{oc}=1.7±0.2, with 158 sites having significantly valid coefficients. On a seasonal basis the coefficients do not vary significantly. Based on estimates reported from other studies and the analysis performed here, we recommend a R_{oc} value of 1.8.

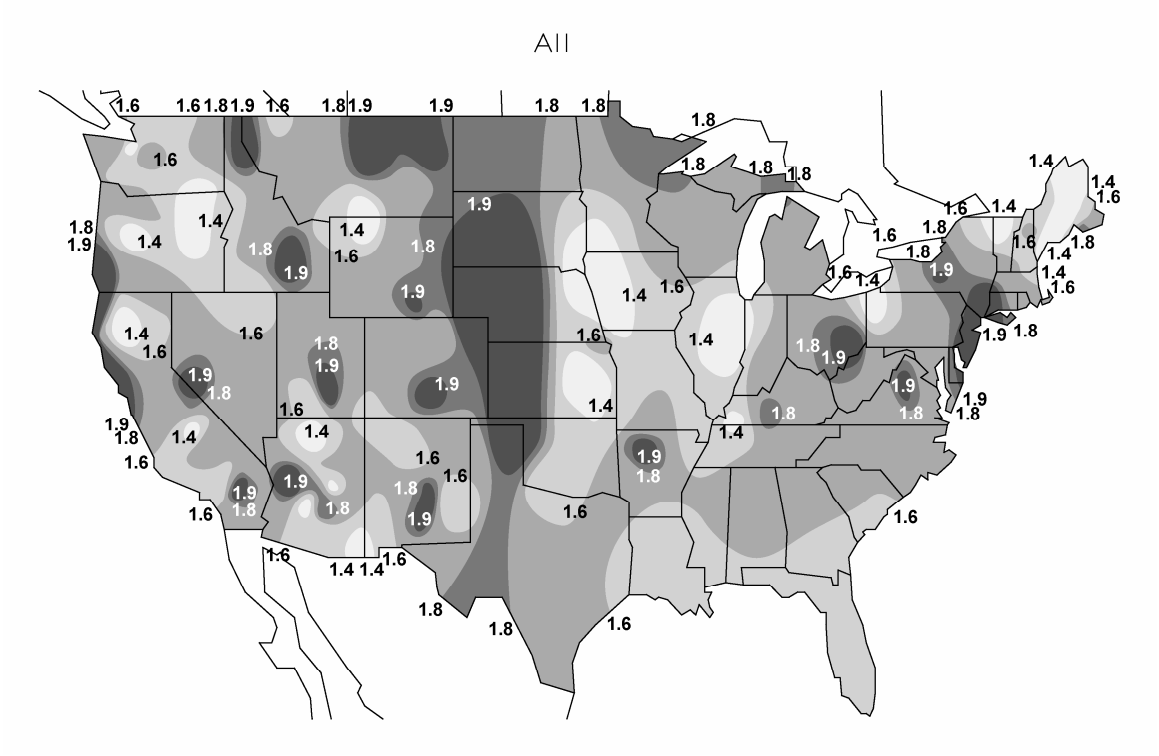

Figure 6.18. Annual mean value of R_{oc} multiplier derived from an ordinary least square multi-linear regression analysis.

6.3.3 Scattering Enhancement Curve (*f(RH)*)

The hygroscopicity of atmospheric aerosols is an important characteristic that determines how a particle will behave in a changing relative humidity (*RH*) environment. Soluble particles will uptake water, resulting in increased mass and particle size, both of which determine how efficiently particles scatter light, as well as their atmospheric lifetimes. A pure salt particle (e.g., ammonium sulfate) exposed to increasing *RH* will undergo an abrupt change from a solid particle to a droplet at a particular relative humidity (referred to as deliquescence) that is specific to its chemical composition. Above this point the particle continues to grow exponentially. As the *RH* decreases, the solution droplet will lose water by evaporation and remain in a metastable supersaturated state until it effloresces and returns to a solid particle at a lower RH than that at which it deliquesced. The metastable state can exist for indefinite periods of time. This behavior is also referred to as hysteresis because the particle follows a different path of growth and evaporation.

It is likely that a large fraction of hygroscopic particles exist in supersaturated equilibrium as aqueous droplets below their deliquescence *RH*, based on the numerous studies that report a smooth function of particle growth with relative humidity rather than step-wise growth behavior. This behavior has been observed for particle growth curves (D/D_o) in southeast Texas (Santarpia et al., 2004, 2005), Great Smoky Mountains National Park (Hand et al., 2000), and Yosemite National Park (Carrico et al., 2005). Smooth *f(RH)* curves have been observed in the Netherlands (ten Brink et al., 1996), Great Smoky Mountains, Grand Canyon, Big Bend, and Yosemite national parks (e.g., Malm and Day, 2001; Malm et al., 2003; 2005b), Portugal

(Carrico et al., 2000), China (Xu et al., 2002), North Carolina (Im et al., 2001), the Maldives (Eldering et al., 2002), and during the Aerosol Characterization Experiment in Asia (ACE-Asia) (Carrico et al., 2003). Although a variety of aerosol types likely exist at these locations, their smooth growth curves suggest these particles exist either in a equilibrium state, lacking growth characteristics like deliquescence points due to their nonsoluble/soluble mixture, or in a supersaturated equilibrium state with a very low efflorescence *RH* (i.e., acidic aerosols). In either case, water appears to be associated with these aerosols at low values of *RH*.

The current *f(RH)* growth curve used in the IMPROVE equation is based on an interpolated D/D_o curve between the ascending and descending branches of growth for ammonium sulfate and reaches a value 1 at 40% *RH* (no water is associated with the particles below 40% *RH*) (Sisler and Malm, 1994). We propose applying an *f(RH)* growth curve corresponding to equilibrium calculations for ammonium sulfate below the deliquescence point to 0% *RH* using the AIM (Aerosol Inorganics Model) model with the "no solids" option (Clegg et al., 1998). This smooth curve approximates the behavior observed for mixtures of aerosols as those observed in the studies cited above; it differs from the current curve in that it allows water to be associated with the aerosol for *RH* values below 40%. The *f(RH)* scattering enhancement curve is consistent with the value of dry mass scattering efficiency used to compute extinction coefficients; therefore modifications made to one parameter must also be made to the other. Organics are assumed to be nonhygroscopic because laboratory and field results suggest they are weakly to nonhygroscopic (Malm et al., 2003, Carrico et al., 2005; Malm et al. 2005b).

6.3.4 Sea Salt

Although contributions from sea salt to coarse mass (and indirectly to fine mass) currently are not included in the reconstructed mass equation, sea salt can be a significant fraction of the fine mass at many coastal locations, (e.g., the Virgin Islands), as well as contribute significantly to light scattering (e.g., Quinn et al., 2001, 2002, 2004). Because sea salt is hygroscopic, the added effects of water mass to light scattering in coastal higher *RH* environments could be important also. Difficulties in computing sea salt from data from the IMPROVE network arise because sodium ion data (the strongest indicator of sea salt) are not available. Elemental sodium data are available from X-ray fluorescence (XRF) analyses; however, sensitivity issues regarding poor detection of Na result in large uncertainties corresponding to Na from XRF (White et al., 2004). Issues also arise when using the chloride ion or chlorine to estimate sea salt because reaction of gaseous nitric acid with sea salt produces sodium nitrate particles and the release of gaseous HCl. The depletion of chloride during this reaction results in an underestimation of sea salt when using chloride to compute it. For noncoastal sites, the inclusion of sea salt is not expected to have a considerable impact on reconstructed light scattering, so underestimating the contribution at those sites is not significant.

The MLR analysis in equation 4 included sea salt as $1.6 \cdot Cl^-$ (NaCl). This analysis suggests that east and west coastal sites underestimate sea salt mass by about 10% on average, even with some chloride depletion. We recommend that sea salt be included in the reconstructed fine mass equation as $1.8 \cdot Cl^-$ (sea salt is 55% Cl by weight as defined by the composition of sea water by Seinfeld and Pandis, 1998) because of the uncertainties related to sodium measurements. A dry sea salt mass scattering efficiency of 1.7 $m^2 g^{-1}$ is recommended, corresponding to a dry lognormal size distribution with geometric mass mean diameter of 2.5

and geometric standard deviation of 2 (Quinn et al.,1996), a refractive index of 1.55, and a density of 1.9 g cm^{-3}. Hygroscopic effects of sea salt are taken into account by applying D/D_o particle growth curves for NaCl (Tang, 1997) and computing *f(RH)* curves with the above assumed size distribution.

6.3.5 Mass Scattering Efficiencies

Estimates of dry mass scattering efficiencies (α_{sp}) depend on the aerosol composition and size distribution, both of which vary temporally and spatially and typically are unknown without extensive measurements. A recent literature review (Hand and Malm, 2006) suggests the current values applied in the IMPROVE formulation are realistic; however, lowering mass scattering efficiencies for inorganic salts would be more consistent with available data. We also suggest that *POM* mass scattering efficiencies should also be decreased; however, at least under some circumstances, the *POM* scattering efficiency is most likely higher than what is currently assumed. We recommend no changes to mass scattering efficiencies for fine soil and coarse mass, nor do we recommend changes to the LAC mass absorption efficiency.

Investigations of estimates of mass scattering efficiency from IMPROVE mass and nephelometry data suggest a functional dependence of mass scattering efficiencies on mass concentrations in that, as mass concentrations increase, mass scattering efficiencies also tend to increase at most sites in an approximately linear fashion (Malm and Hand, 2006). This functional dependence is accounted for by assuming a bimodal size distribution. The smaller size mode corresponds to lower mass scattering efficiencies under low mass concentration conditions associated with younger particles. The large size mode corresponds to higher values of α_{sp} for higher mass concentration conditions assumed to be associated with aged or cloud-processed aerosols. The size modes are described by lognormal size distributions with geometric mass mean diameters and geometric standard deviations of 0.2 μm and 2.2 for the small mode and 0.5 μm and 1.5 for the large mode, respectively, and are assumed for ammonium sulfate, ammonium nitrate, and *POM*. The annual mean ammonium sulfate mass scattering efficiency is shown in Figure 6.19. Values tend to be lower in the Southwest compared to the eastern United States, ranging from 2.27 $m^2 g^{-1}$ in Jarbidge Wilderness NV (JARB) to 3.11 $m^2 g^{-1}$ in Mammoth Cave National Park KY (MACA), with a mean and standard deviation for all sites of 2.5±0.3 $m^2 g^{-1}$. The annual mean POM mass scattering efficiency for all sites is shown in Figure 6.20. The average (and one standard deviation) of all sites is 3.2±0.2 $m^2 g^{-1}$, ranging from 2.9 $m^2 g^{-1}$ in the Virgin Islands (VIIS) (not shown) to 3.71 $m^2 g^{-1}$ in Phoenix AZ (PHOE).

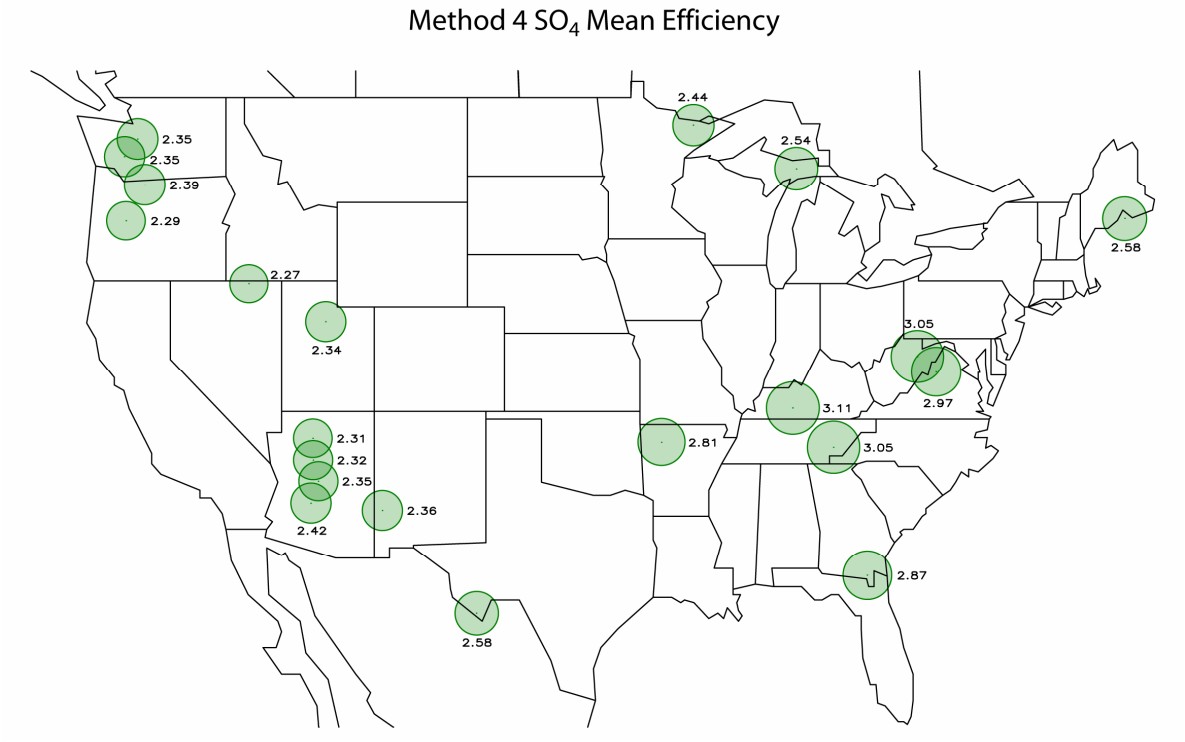

Figure 6.19. Map of the mean ammonium sulfate mass scattering efficiency (m^2 g^{-1}). The size of the circle reflects the magnitude of the efficiency, which is printed near the circle.

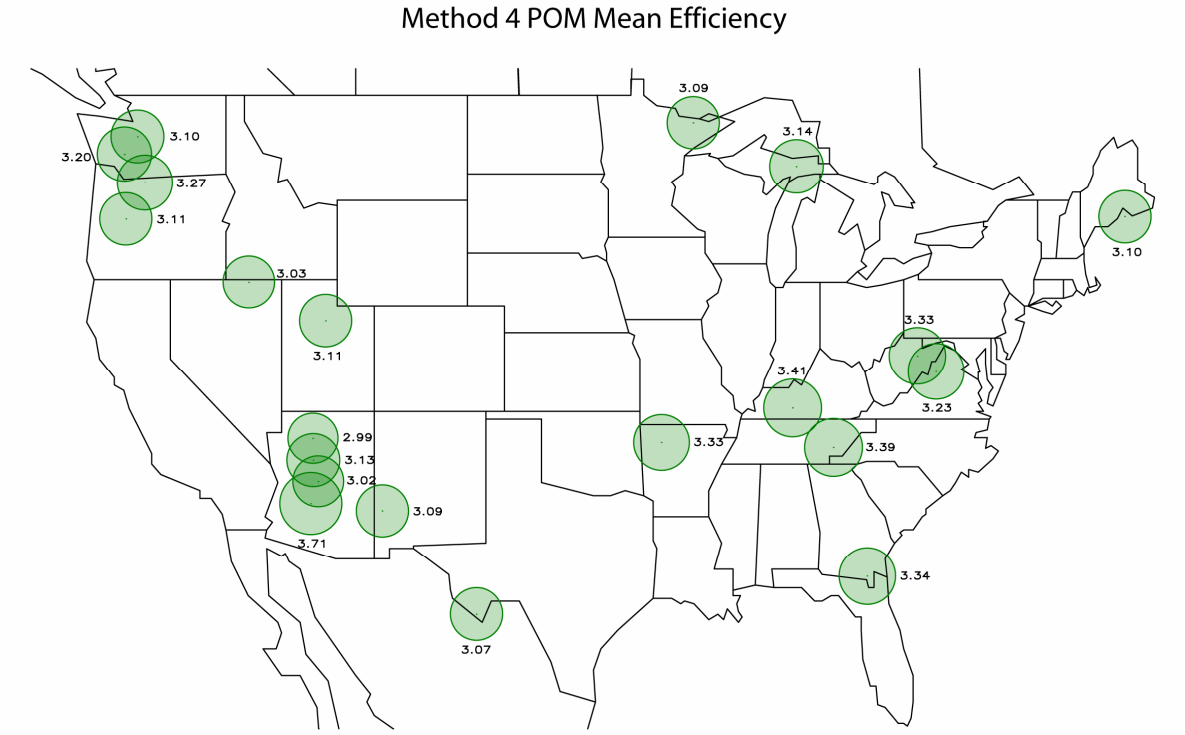

Figure 6.20. Map of the mean POM mass scattering efficiency (m^2 g^{-1}). The size of the circle reflects the magnitude of the efficiency, which is printed near the circle.

6.3.6 Site-Specific Rayleigh Scattering

The current IMPROVE equation assumes a constant value of 10 Mm^{-1} regardless of location. Rayleigh scattering depends on air density and varies with temperature and pressure. For each IMPROVE site b_{ray} was computed using the standard atmospheric pressure corresponding to the site elevation and the annual mean temperature. Values range from 8 Mm^{-1} for sites elevations around 12,000 feet to 12Mm^{-1} for sites near sea level.

6.3.7 Light Absorption by NO_2

The NO2 absorption efficiency is computed using equation 5:

$$PAE_{NO_2} = \frac{\sum_{350}^{750} PR(\lambda) \times AE(\lambda)}{\sum_{350}^{750} PR(\lambda)} \qquad (5)$$

where the NO_2 absorption efficiency ($AE(\lambda)$) is multiplied by the relative observer photopic response ($PR(\lambda)$) for viewing an image of 2º angular size (Dixon, 1940). This product is summed over the wavelengths from 350 to 750 nm and divided by the sum of the photopic response over the same wavelength range. The NO_2 absorption efficiency is 0.33 Mm^{-1}/ppb.

6.3.8 New IMPROVE Equation

The new IMPROVE equation is proposed as

$$\begin{aligned} b_{ext} = {} & 2.2 \cdot f_S(RH) \cdot [(NH_4)_2 SO_4]_S + 4.8 \cdot f_L(RH) \cdot [(NH_4)_2 SO_4]_L \\ & + 2.4 \cdot f_S(RH) \cdot [NH_4NO_3]_S + 5.1 \cdot f_L(RH) \cdot [NH_4NO_3]_L \\ & + 2.8 \cdot [POM]_S + 6.1 \cdot [POM]_L \\ & + 10 \cdot [LAC] \\ & + 1.0 \cdot [Soil] \\ & + 1.7 \cdot f_{SS}(RH) \cdot [Seasalt] \\ & + 0.6 \cdot [CM] \\ & + b_{ray} \\ & + 0.33 \cdot [NO_2(ppb)] \end{aligned}$$

where

$$[(NH_4)SO_4]_L = \frac{[total\ (NH_4)SO_4]}{20} \cdot [total\ (NH_4)SO_4],\ for\ [total\ (NH_4)SO_4] < 20\ \mu g\ m^{-3}$$

$$\left[(NH_4)SO_4\right]_L = \left[total\ (NH_4)SO_4\right],\ for\ \left[total\ (NH_4)SO_4\right] \geq 20\ \mu g\ m^{-3}$$

$$\left[(NH_4)SO_4\right]_S = \left[total\ (NH_4)SO_4\right] - \left[\ (NH_4)SO_4\right]_L$$

Similar equations hold for ammonium nitrate and POM.

For a more comprehensive review of the IMPROVE equation, download the final report at http://vista.cira.colostate.edu/improve/Publications/GrayLit/016_IMPROVEeqReview/IMPROVEeqReview.htm

References

Andrews, E., P. Saxena, S. Musarra, L. M. Hildemann, P. Koutrakis, P. H. McMurry, I. Olmez, W. H. White, Concentration and composition of atmospheric aerosols from the 1995 SEAVS experiment and a review of the closure between chemical and gravimetric measurements, *J. Air & Waste Manage. Assoc., 50,* 648-664, May 2000.

Carrico, C. M., M. J. Rood, J. A. Ogren, C. Neusüß, A. Wiedensohler, and J. Heintzenberg, Aerosol optical properties at Sagres, Portugal during ACE-2, *Tellus, 52B,* 694-715, 2000.

Carrico, C. M., M. H. Bergin, J. Xu, K. Baumann, and H. Maring, Urban aerosol radiative properties: Measurements during the 1999 Atlanta Supersite Experiment, *J. Geophys. Res., 108(D7)*, 8422, doi:10.1029/2001JD001222, 2003.

Carrico, C. M., S. M. Kreidenweis, W. C. Malm, D. E. Day, T. Lee, J. Carrillo, G. R. McMeeking, and J. L. Collett, Jr., Hygroscopic growth behavior of a carbon-dominated aerosol in Yosemite National Park, *Atmos. Environ., 39*, 1393-1404, 2005.

Clegg S.L., P. Brimblecombe, and A.S. Wexler, A thermodynamic model of the system H+-NH4+-Na+-SO42—NO3—Cl—H2O at 298.15 K, *J. of Phys. Chem.102A*, 2155-2171, 1998.

Countess, R. J., G. T. Wolff, and S. H. Cadle, The Denver winter aerosol: A comprehensive chemical characterization, *J. Air Pollution Control Assoc., 30,* 1194-1200, 1980.

Dixon, J. K., The absorption coefficient of nitrogen dioxide in the visible spectrum, *J. Chem. Phys., 8(2),* 157-160, 1940.

Eldering, A., J. A. Ogren, Z. Chowdhury, L. S. Hughes, and G. R. Cass, Aerosol optical properties during INDOEX based on measured aerosol particle size and composition, *J. Geophys. Res.,107(D22),* 8001, doi:10.1029/2001JD001572, 2002.

El-Zanan, H. S., D. H. Lowenthal, B. Zielinska, J. C. Chow, and N. Kumar, Determination of the organic aerosol mass to organic carbon ratio in IMPROVE samples, *Chemosphere, 60(4),* 485-496, 2005.

Grosjean, D., and S. K. Friedlander, Gas-particle distribution factors for organics and other pollutants in the Los Angeles atmosphere, *J. Air Pollution Control Assoc., 25,* 1038-1044, 1975.

Hand, J. L., R. B. Ames, S. M. Kreidenweis, D. E. Day and W. C. Malm, Estimates of particle hygroscopicity during the Southeastern Aerosol and Visibility Study, *J. Air & Waste Manage. Assoc., 50,* 677-685, May 2000.

Hand, J. L., and W. C. Malm, Review of the IMPROVE equation for estimating ambient light extinction coefficients (final report), http://vista.cira.colostate.edu/improve/Publications/GrayLit/016_IMPROVEeqReview/IMPROVEeqReview.htm, 2005.

Hand, J. L., and W. C. Malm, Review of aerosol mass scattering efficiencies from ground-based measurements since 1990, *In preparation for submission to J. Geophysical Res.,* 2006.

Im, J.-S., V. K. Saxena, and B. N. Wenny, An assessment of hygroscopic growth factors for aerosols in the surface boundary layer for computing direct radiative forcing, *J. Geophys. Res., 106(D17)*, 20213-20224, 2001.

Japar, S. M., A. C. Szkarlat, R. A. Gorse, Jr., E. K. Heyerdahl, R. L. Johnson, J. A. Rau, and J. J. Huntzicker, Comparison of solvent extraction and thermal optical carbon analysis methods: Application to diesel vehicle exhaust aerosol, *Environ. Sci. Techonol., 18,* 231-234, 1984.

Malm, W. C., J. F. Sisler, D. Huffman, R. A. Eldred, and T. A. Cahill, Spatial and seasonal trends in particle concentration and optical extinction in the United States, *J. Geophys. Res., 99(D1)*, 1347-1370, 1994.

Malm W.C. and D. E. Day, Estimates of aerosol species scattering characteristics as a function of relative humidity, *Atmos. Environ., 35,* 2845-2860, 2001.

Malm W.C., D. E. Day, S. M. Kreidenweis, J. L. Collett, Jr., T. Lee, T., Humidity dependent optical properties of fine particles during the Big Bend Regional Aerosol and Visibility Observational study (BRAVO), *J. Geophys. Res. 108(D9),* 4279, doi:10.1029/2002JD002998, 2003.

Malm W.C., D. E. Day, C. Carrico, S. M. Kreidenweis, J. L. Collett, Jr., G. McMeeking, T. Lee, J. Carrillo, Inter-comparison and closure calculations using measurements of aerosol species and optical properties during the Yosemite Aerosol Characterization Study, *J. Geophys. Res., 110,* D14302, doi:10.1029/2004JD005494*,* 2005a.

Malm, W. C., D. E. Day, S. M. Kreidenweis, J. L. Collett, Jr., C. Carrico, G. McMeeking, and T. Lee, Hygroscopic properties of organic-laden aerosol*, Atmos. Environ., 39,* 4969-4982, 2005b.

Malm, W. C. and Hand, J. L., An examination of aerosol physical and optical properties collected in the IMPROVE program, *Submitted to Atmos. Environ.,* 2006.

Poirot, R. L. and R. B.Husar, Chemical and physical characteristics of wood smoke in the northeastern U.S. during July 2002: Impacts from Quebec forest fires, Paper # 94, A&WMA Specialty conference: Regional and Global Perspectives on Haze: Causes, Consequences and Controversies, Asheville, NC, October 25-29, 2004.

Quinn, P. K., V. N. Kapustin, T. S. Bates and D. S. Covert, Chemical and optical properties of marine boundary layer aerosol particles of the mid-Pacific in relation to sources and meteorological transport, *J. Geophys. Res., 101(D3),* 6931-6951, 1996.

Quinn, P. K., D. J. Coffman, T. S. Bates, T. L. Miller, J. E. Johnson, K. Voss, E. J. Welton, and C. Neususs, Dominant aerosol chemical components and their contribution to extinction during the Aerosols99 cruise across the Atlantic, *J. Geophys. Res., 106(D18)*, 20783-20809, 2001.

Quinn, P. K., D. J. Coffman, T. S. Bates, T. L. Miller, J. E. Johnson, E. J. Welton, C. Neususs, M. Miller, and P. J. Sheridan, Aerosol optical properties during INDOEX 1999: Means, variability, and controlling factors, J. Geophys. Res., *107(D19), 8020,* doi:10.1029/2000JD000037, 2002.

Quinn, P. K., D. J. Coffman, T. S. Bates, E. J. Welton, D. S. Covert, T. L. Miller, J. E. Johnson, S. Maria, L. Russell, R. Arimoto, C. M. Carrico, M. J. Rood, and J. Anderson, Aerosol optical properties measured on board the *Ronald H. Brown* during ACE-Asia as a function of aerosol chemical composition and source region, *J. Geophys. Res., 109(D19S01)*, doi:10.1029/2003JD004010, 2004.

Santarpia, J. L., R. Li, and D. R. Collins, Direct measurement of the hydration state of ambient aerosol populations, *J. Geophys. Res.,109,* D18209*,* doi:10.1029/2004.

Santarpia, J. L., R. Gasparini, R. Li, and D. R. Collins, Diurnal variations in the hygroscopic growth cycles of ambient aerosol populations, *J. Geophys. Res.,110,* D03206, doi:10.1029/2004JD005279, 2005.

Seinfeld, J. H. and S. N. Pandis, *Atmospheric Chemistry and Physics: From Air Pollution to Climate Change,* John Wiley, New York, pp 444, 1998.

Sisler, J. F. and W. C. Malm, The relative importance of soluble aerosols to spatial and seasonal trends of impared visibility in the United States, *Atmos. Environ., 28(5),* 851-862, 1994.

Tang, I. N., Thermodynamic and optical properties of mixed-salt aerosols of atmospheric importance, *J. Geophys. Res.,102(D2),* 1883-1893, 1997.

ten Brink, H. M., J. P. Veefkind, A. Waijers-Ijpelaan, and J. C. Van der Hage, Aerosol light scattering in the Netherlands, *Atmos. Environ., 30(24),* 4251-4261, 1996.

Turpin, B. J., and H.-J. Lim, Species contributions to $PM_{2.5}$ mass concentrations: Revisiting common assumptions for estimating organic mass, *Aerosol Sci. Technol., 35,* 602-610, 2001.

Van Vaeck, L. and K. Van Cauwenberghe, Cascade impactor measurements of the size distribution of the major classes of organic pollutants in atmospheric particulate matter, *Atmos. Environ., 12,* 2239, 1978.

White, W. H. and P. T. Roberts, On the nature and origins of visibility-reducing aerosols in the Los Angels Air Basin, *Atmos. Environ., 11,* 803-812, 1977.

White, W. H., R. A. Eldred, P. J. Feeney, C. E. McDade, B. P. Perley, D. J. Shadoan, and P. H. Wakabayashi, Behavior of fine-particle elemental data near the detection limit, Paper # 24, A&WMA Specialty conference: Regional and Global Perspectives on Haze: Causes, Consequences and Controversies, Asheville, NC, October 25-29, 2004.

Xu, J., M. H. Bergin, X. Yu, G. Liu, J. Zhao, C. M. Carrico, and K. Baumann, Measurement of aerosol chemical, physical and radiative properties in the Yangtze delta region of China, *Atmos. Environ., 36,* 161-173, 2002.

6.4 COARSE PARTICLE SPECIATION AT SELECTED LOCATIONS IN THE RURAL CONTINENTAL UNITED STATES

Abstract

A few short-term special studies at national parks have shown that coarse mass (2.5–10 μm) may not be just crustal minerals but may consist of a substantial amount (≈ 40–50%) of carbonaceous material and inorganic salts such as calcium nitrate and sodium nitrate. To more fully investigate the composition of coarse particles, a program of coarse particle sampling and speciation analysis at nine of the IMPROVE sites was initiated 19 March 2003 and operated through the year 2004. Only the data for 2004 are reported here. Sites were selected to be representative of the continental United States and were operated according to IMPROVE protocol analytic procedures. Crustal minerals (soil) are the single largest contributor to coarse mass (CM) at all but one monitoring location. The average fractional contributions range from a high of 76% at Grand Canyon National Park to a low of 34% at Mount Rainier National Park. The second largest contributor to CM is organic mass, which on an average annual fractional basis is highest at Mount Rainier at 59%. At Great Smoky Mountains National Park, organic mass contributes 40% on average, while at four sites organic mass concentrations contribute between 20% and 30% of the CM. Nitrates are on average the third largest contributor to CM concentrations. The highest fractional contributions of nitrates to CM are at Brigantine National Wildlife Refuge, Great Smoky Mountains, and San Gorgonio wilderness area at 10–12%. Sulfates contribute less than about 5% at all sites.

6.4.1 Introduction

The Regional Haze Rule (U.S. Environmental Protection Agency, 1999) requires monitoring representative of 156 visibility-protected federal areas (VPFAs) beginning in January 2001. This entails particle sampling and analysis of the major aerosol components using methods patterned after those utilized since 1987 by the Interagency Monitoring of Protected Visual Environments (IMPROVE) network (Joseph, et al., 1987; Malm et al., 1994).

In 1999, the IMPROVE network consisted of 30 monitoring sites in VPFAs, 20 of which began operation in 1988, with the others starting in the early 1990s. About this time the EPA provided supplemental support to expand the network to about 110 monitoring sites. Additional information about the site selection process is available elsewhere (Malm et al., 2000a; Colorado State University, http://vista.cira.colostate.edu/improve/).

The aerosol data collected in the IMPROVE program have been widely analyzed to better understand the seasonal and spatial patterns of fine aerosol components and their contribution to light extinction (Eldred et al., 1993; Malm et al., 1994; Sisler and Malm, 2000; Malm et al., 2004). The spatial patterns of trace elements, e.g., selenium, vanadium, zinc, and bromine have also been examined (Eldred, 1997; Malm and Sisler, 2000). At sites where more than 10 years of data were collected, temporal trends in fine mass (FM) and its major aerosol components have been examined (Iyer et al., 2000; Patterson et al., 2000; Malm and Sisler, 2000; Malm et al., 2002).

However, fine particles (< 2.5 μm) are speciated, while coarse particles (2.5–10.0 μm) are not. A few short-term special studies at national parks have shown that coarse mass (CM) is not just crustal minerals but consists of a substantial amount (≈ 40–50%) of carbonaceous material and inorganic salts such as calcium nitrate and sodium nitrate (Malm and Day, 2000; Lee et al., 2004; Malm et al., 2005). To more fully investigate the composition of coarse particles, a program of coarse particle sampling and speciation analysis at nine of the IMPROVE sites was initiated between 19 March 2003 and 23 December 2003 and operated through the year 2004. Only data from the year 2004 are reported here. Sites were selected to be representative of the continental United States and are listed in Table 6.1, along with the fine particle monitoring start date, elevation, and location of each of the sites. This paper reports on monthly trends in speciated FM and CM concentrations derived from data collected during 2004 at these sites and compares them to historical trends.

Table 6.1. Site description.

Site	Elevation (M)	State	Latitude (Degrees)	Longitude (Degrees)	Start Date
Bondville	211	Illinois	40.0514	-88.3719	3/5/2001
Bridger wilderness area	2607	Wyoming	42.9749	-109.757	3/2/1988
Brigantine National Wildlife Refuge	5	New Jersey	39.465	-74.4492	9/18/1991
Grand Canyon National Park	2267	Arizona	35.9731	-111.984	3/12/1988
Great Smoky Mountains National Park	815	Tennessee	35.6334	-83.9417	3/2/1988
Mount Rainier National Park	427	Washington	46.7579	-122.123	3/2/1988
San Gorgonio wilderness area	1705	California	34.1924	-116.901	3/2/1988
Sequoia National Park	535	California	36.4894	-118.829	3/4/1992
Upper Buffalo wilderness area	723	Arkansas	35.8259	-93.2029	12/18/1991

6.4.2 Particulate Samplers

The basic IMPROVE sampler was designed for the IMPROVE network and has been operated extensively in the network and during field studies since the winter of 1987 (Malm et al., 1989; Malm et al., 1994). The IMPROVE sampler consists of four independent modules. Each module incorporates a separate inlet, filter pack, and pump assembly; however, all modules are controlled by the same timing mechanism. Twice-weekly 24-h duration samples are collected using the same schedule as the national particulate matter (PM) monitoring network operated by state and local governments.

The sampler has a four-filter manifold for each module. Modules A, B, and C are each equipped with a 2.5 μm cyclone. The module A Teflon filter is analyzed for gravimetric FM, nearly all elements with atomic mass number ≥ 11 (Na) and ≤ 82 (Pb) by x-ray florescence (XRF), elemental hydrogen by proton elastic scattering analysis, and for light absorption. For module B, the sampled air is drawn through a sodium carbonate denuder tube in the inlet to remove gaseous nitric acid; the material collected on the Nylasorb substrate is extracted ultrasonically in a de-ionized water bath and subsequently analyzed by ion chromatography for the anions sulfate, nitrate, nitrite, and chloride. Module C utilizes quartz fiber filters for the collection of fine particles that are subsequently analyzed for carbon. At some sites, tandem quartz filters are used so that the second filter is available for estimating the organic carbon artifact associated with hydrocarbon gases trapped in the filter substrate. Thermal optical

reflectance (TOR) is the analytical technique used for determination of organic and elemental/light-absorbing carbon (LAC) (Chow et al., 1993). Finally, module D, fitted with a PM_{10} inlet, utilizes a Teflon filter that is gravimetrically analyzed for mass (PM_{10}). In this study, a second set of modules B and C were operated with a PM_{10} inlet (and denoted modules E and F). These and the Teflon filter from the D module were analyzed, allowing for an estimate of species mass in the 2.5–10.0 μm range. It is this size range that will be referred to as the coarse mode.

6.4.3 Estimation of Aerosol Mass

The fine and coarse aerosol species concentrations at most continental sites can be classified into six major types: sulfates, nitrates, organics, LAC, crustal minerals (often referred to as soil), and sea salt. Details of standard methods for apportionment of measured mass to the various aerosol species concentrations are described in some detail in Malm et al. (1994), while Table 6.2 presents the standard equations currently used in the IMPROVE program for estimating the species concentrations.

Table 6.2. Assumed molecular forms of each particulate species and method of estimation used.

Species	Formula	Assumptions
Sulfate	4.125[S] or 1.37*[SO_4^{--}]	All elemental S is from sulfate. All sulfate is from ammonium sulfate.
Nitrate	1.29[NO_3^-]	Denuder efficiency is close to 100%. All nitrate is from ammonium nitrate.
LAC (light-absorbing carbon by channel C)	[EC1]+[EC2]+[EC3]-[OP]	All high temp carbon is elemental
OMC (Organic mass from carbon)	1.8{[O1]+[O2]+[O3]+[O4]+[OP]}	Average organic molecule is 56% carbon.
SOIL	2.2[Al]+2.19[Si] +1.63[Ca]+2.42[Fe] +1.94[Ti]	[Soil K]=0.6[Fe]. FeO and Fe_2O_3 are equally abundant. A factor of 1.16 is used for MgO, Na_2O, H_2O, CO_2
Sea salt	1.8*[Cl^-]	1.8 accounts for other salts than NaCl
RCFM (reconstructed fine mass)	[SULFATE]+[NITRATE] +[LAC]+[OMC]+[SOIL] +[SEA SALT]	Represents dry ambient fine aerosol mass for continental sites.
Coarse mass species	[PM_{10}] species - [$PM_{2.5}$] species	Difference between species found on the <10 μm and 2.5 μm substrates—coarse and fine species have same chemical form.

A number of measurement programs have shown that, during summer months in the eastern United States, the average sulfate ammoniation is nearer ammonium bisulfate, with ammonium-to-sulfate molar ratios that can approach sulfuric acid (Gebhart et al., 1994; Malm et al., 2000b; Lefer and Talbot, 2001). Measurements at Big Bend, Texas, showed ammonium-to-sulfate molar ratios of about 1.4 on average (Malm et al., 2003). However, because the ammonium ion is not routinely measured in the IMPROVE program, sulfates will be assumed to

be in the form of ammonium sulfate for the purpose of examining general spatial and temporal trends in sulfate mass concentrations.

Nitrates in the aerosol are assumed to be in the form of ammonium nitrate, but, again, special studies have shown that at some locations fine nitrates are the fine tail of the coarse particle nitrate size distribution, consisting of sodium nitrate or calcium nitrate, that has resulted from the reaction of nitric acid vapor with sea salt or crustal minerals (Malm et al., 2003). Assuming nitrates are in the molecular form of ammonium nitrate would underestimate nitrate mass concentrations by about 6% and by a factor of 2 if the true molecular compositions were sodium nitrate and calcium nitrate, respectively.

An average ambient particulate organic compound is assumed to have a constant fraction of carbon by weight. Particulate organic carbon mass concentration (POM) from module C is assumed to be [POM] = 1.8[OC], where OC is organic carbon as determined by TOR. The factor of 1.8 corrects the organic carbon mass for other elements associated with the assumed organic molecular composition (Turpin and Lim, 2001; Poirot and Husar, 2004; Malm et al., 2005; Malm and Hand, 2006).

Concentrations of crustal minerals, referred to as soil, are estimated by summing the elements predominantly associated with common crustal elements measured by XRF plus oxygen for the compounds (Al_2O_3, SiO_2, CaO, K_2O, FeO, Fe_2O_3, TiO_2) and applying an adjustment to account for other unmeasured compounds such as MgO, Na_2O, water, and carbonate.

Sea salt concentrations are typically computed from sea salt markers such as the sodium ion, chloride ion, or combination of ions (Quinn et al., 2001). Difficulties in computing sea salt from data from the IMPROVE network arise because positive ions are not analyzed; therefore sodium ion (the strongest indicator of sea salt) data are not available. Elemental sodium data are available from XRF analyses; however, sensitivity issues regarding poor detection of Na result in large uncertainties (White et al., 2004). Issues also arise when using the chloride ion or chlorine to estimate sea salt, because reaction of gaseous nitric acid with sea salt produces sodium nitrate particles and the release of gaseous HCl. The depletion of chloride during this reaction results in an underestimation of sea salt when using chloride to compute it. However, because the chloride ion is the only accurately measured marker for sea salt in the IMPROVE program, $1.8[Cl^-]$ will be used to estimate sea salt concentrations (sea salt is 55% Cl by weight as defined by the composition of sea water by Seinfeld and Pandis, 1998).

The self-consistency and overall quality of the measurements are assured by redundancy and intercomparisons between independently measured species. A description of validation and quality assurance procedures is available in Eldred et al. (1988), Sisler et al. (1993), and Malm et al. (1994). In the most general sense, validation is a matter of comparing chemically related species that have been measured in different modules. Fortunately, the design of the IMPROVE sampler allows for redundancy between certain module A measurements and module B and C measurements of the ions and carbons, enabling quality control checks. For example, elemental sulfur mass × 3 should agree with the sulfate ion measured in module B. Reconstructed fine mass (RCFM), defined and used in this paper as the sum of the individual species described above, should agree with measurements of gravimetric mass. However, when comparing gravimetric

FM to RCFM, a number of complicating factors must be dealt with. First, under some conditions, a large portion of the nitrates (≥ 50%) can volatilize from the module A Teflon filter. Second, because of water retention by soluble aerosol species, the amount of residual water on the filter is a function of the relative humidity (RH) at which the filter was weighed and the history of the RH to which the aerosol was exposed.

6.4.4 The Data Set

The combined FM and CM concentration data sets for the 2004 year of monitoring at the nine sites are summarized in Tables 6.3 and 6.4 as the mean, standard deviation, maximum, and minimum for each species measured. Also shown in the last column is the fraction of gravimetric mass for each species. There are a total of 1014 data points. Reconstructed mass is the sum of all species. Negative values occur for the FM species because filter blanks exceed measured values, while for the CM species, negative values are also associated with reported PM_{10} mass concentrations for a given species that are less than $PM_{2.5}$ mass concentrations. For FM, the mean reconstructed value is 7% greater than the mean measured mass, while for CM the mean reconstructed value is 3% less than the mean measured mass. Scatter plots of reconstructed versus measured FM and CM are presented in Figs. 6.21 and 6.22. For both data sets, the agreement is quite good. However, for the FM data set, reconstructed mass tends to be overestimated in the mid-range mass concentration values of 5–12 μg m^{-3}, and there is substantially more scatter around the 1:1 line for the CM than for the FM data set. With the intercept forced through 0, the ordinary least square (OLS) slopes for the data shown in Figs. 6.21 and 6.22 are 1.03 ± .004 and 0.95 ± .01, respectively. Corresponding R^2 values are 0.96 and 0.81.

Table 6.3. Statistical summary of all fine mass and fine mass species concentrations.

Variable (μg m^{-3})	Mean	Std. Dev.	Minimum	Maximum	% of FM
FM	6.64	5.44	0.09	39.75	
FM_{RECON}	7.12	5.49	0.19	36.00	107.2
$(NH_4)_2SO_4$	2.70	3.08	0.02	21.74	40.7
NH_4NO_3	1.19	2.07	0.00	27.97	17.9
POM	2.32	1.90	-0.03	14.17	34.9
LAC	0.27	0.20	0.01	2.07	4.1
SOIL	0.62	0.69	0.01	6.89	9.3
Sea salt	0.02	0.13	0.00	2.13	0.3

Table 6.4. Statistical summary of all coarse mass and coarse mass species concentrations.

Variable (μg m^{-3})	Mean	Std. Dev.	Minimum	Maximum	% of CM
CM	5.24	5.81	-1.75	49.93	
CM_{RECON}	5.07	5.97	-3.47	46.70	96.8
$(NH_4)_2SO_4$	0.03	0.50	-4.23	4.54	0.6
NH_4NO_3	0.41	0.50	-1.72	2.97	7.8
POM	1.28	1.41	-3.35	15.29	24.4
LAC	0.07	0.13	-0.54	1.52	1.3
SOIL	3.19	4.87	-0.02	39.73	60.9
Sea salt	0.10	0.51	-0.11	6.99	1.9

On the average, sulfate interpreted as ammonium sulfate and POM make up 41% and 35% of the FM, respectively, while ammonium nitrate contributes another 18%. Soil mass concentration is less than 10% of measured mass, LAC about 4%, and sea salt is negligible. For the CM fraction, the sulfate contribution is negligible and LAC and sea salt are only 1% and 2%, respectively. As expected, crustal minerals (soil) are the major component at 61%, but POM and ammonium nitrate contribute significantly at 24% and 8%, respectively.

6.4.5 Spatial Variability of Coarse and Fine Monthly Patterns in Species Mass Concentrations

Statistical summaries of FM and CM aerosol constituents in the form of averages, standard deviations, maximums, and minimums for data aggregations for the year 2004 are shown in Tables 6.5 and 6.6. Also presented in the tables are the percent contribution of each species to gravimetric mass and a comparison of gravimetric and reconstructed mass in the form of a percentage of reconstructed to gravimetric mass. These same summaries are available on a monthly basis at http://vista.cira.colostate.edu/IMPROVE/Data/Other/Data_CMSpeciation.htm. Figs. 6.23 and 6.24 present graphical summaries of these data in the form of average monthly concentrations as stacked bar plots, while Figs. 6.25 and 6.26 show the average fractional contribution of each species to gravimetric FM and CM. The sum of the fractional contributions of each species should sum to 1. Therefore, values greater or less than 1 show the over- or underestimation of reconstructed mass as compared to gravimetric mass. Also, for purposes of comparing the current data set to the historical record, selected average species concentrations are also presented in Figs. 6.23 and 6.24. In the case of FM (Fig. 6.23), historical averages of gravimetric mass and the main constituents of FM—ammonium sulfate, POM, and, in some cases, ammonium nitrate—mass concentrations are plotted. Because only values of coarse gravimetric mass have been routinely measured, only historic values of this variable are presented (Fig. 6.24).

Table 6.5. Statistical summary of annual fine mass and fine mass species concentrations by site.

Mount Rainier Fine Mass	N = 114				
Variable (μg m^{-3})	Mean	Std. Dev.	Minimum	Maximum	% of FM
FM	3.69	2.79	0.09	15.47	
FM_{RECON}	3.92	3.03	0.2	17.45	106.2
$(NH_4)_2SO_4$	0.91	0.71	0.02	2.9	24.7
NH_4NO_3	0.2	0.23	0	1.13	5.4
POM	2.27	2.06	-0.03	12.98	61.5
LAC	0.26	0.2	0.01	0.89	7.0
SOIL	0.25	0.3	0.01	1.45	6.8
Sea salt	0.04	0.11	0	0.67	1.1
San Gorgonio Fine Mass	N = 116				
Variable (μg m^{-3})	Mean	Std. Dev.	Minimum	Maximum	% of FM
FM	5.82	3.48	0.21	14.57	
FM_{RECON}	7.41	4.47	0.63	16.76	127.3
$(NH_4)_2SO_4$	1.6	1.13	0.09	5.83	27.5
NH_4NO_3	2.66	2.22	0.03	9.28	45.7
POM	2.03	1.38	0.15	8.21	34.9

LAC	0.29	0.16	0.05	0.82	5.0
SOIL	0.83	0.69	0.01	3.35	14.3
Sea salt	0	0	0	0.03	0.0
Sequoia Fine Mass	N = 112				
Variable ($\mu g\ m^{-3}$)	Mean	Std. Dev.	Minimum	Maximum	% of FM
FM	8.06	5.4	0.71	39.75	
FM_{RECON}	9.02	5.38	0.99	36	111.9
$(NH_4)_2SO_4$	1.99	1.39	0.13	6.69	24.7
NH_4NO_3	2.14	3.47	0.07	27.97	26.6
POM	3.49	1.94	0.55	8.85	43.3
LAC	0.33	0.16	0.04	0.83	4.1
SOIL	1.07	0.95	0.02	3.45	13.3
Sea salt	0	0	0	0.01	0.0
Grand Canyon Fine Mass	N = 116				
Variable ($\mu g\ m^{-3}$)	Mean	Std. Dev.	Minimum	Maximum	% of FM
FM	2.58	1.94	0.27	14.2	
FM_{RECON}	2.71	2.38	0.19	18.38	105.0
$(NH_4)_2SO_4$	0.8	0.43	0.09	2.57	31.0
NH_4NO_3	0.22	0.26	0.02	2.19	8.5
POM	1.02	1.74	-0.01	14.17	39.5
LAC	0.12	0.22	0.01	2.07	4.7
SOIL	0.55	0.5	0.01	2.37	21.3
Sea salt	0	0	0	0.02	0.0
Upper Buffalo Fine Mass	N = 106				
Variable ($\mu g\ m^{-3}$)	Mean	Std. Dev.	Minimum	Maximum	% of FM
FM	8.1	4.9	1.15	28.84	
FM_{RECON}	8.49	4.78	1.35	26.54	104.8
$(NH_4)_2SO_4$	3.42	2.37	0.38	11.01	42.2
NH_4NO_3	1.16	1.64	0.1	10.43	14.3
POM	2.88	2.25	0.56	13.83	35.6
LAC	0.27	0.16	0.07	1.05	3.3
SOIL	0.76	1.05	0.01	6.89	9.4
Sea salt	0	0	0	0.01	0.0
Bondville Fine Mass	N = 102				
Variable ($\mu g\ m^{-3}$)	Mean	Std. Dev.	Minimum	Maximum	% of FM
FM	10.25	5.72	3.33	33.56	
FM_{RECON}	10.53	5.48	3.24	34.38	102.7
$(NH_4)_2SO_4$	4.26	3.26	0.68	19.84	41.6
NH_4NO_3	2.74	3.11	0.19	24.5	26.7
POM	2.59	1.5	0.51	9.52	25.3
LAC	0.37	0.19	0.11	0.98	3.6
SOIL	0.56	0.34	0.06	1.78	5.5
Sea salt	0	0.02	0	0.12	0.0

Great Smoky Mountains Fine Mass	N = 112				
Variable (μg m^{-3})	Mean	Std. Dev.	Minimum	Maximum	% of FM
FM	10.42	6.06	0.97	28.36	
FM_{RECON}	10.47	5.37	1.55	24.96	100.5
$(NH_4)_2SO_4$	5.87	4.09	0.72	17.64	56.3
NH_4NO_3	0.62	0.77	0.09	4.95	6.0
POM	3.04	1.58	0.37	9.8	29.2
LAC	0.33	0.15	0.07	0.87	3.2
SOIL	0.61	0.58	0.03	4.3	5.9
Sea salt	0	0	0	0	0.0
Bridger Fine Mass	N = 122				
Variable (μg m^{-3})	Mean	Std. Dev.	Minimum	Maximum	% of FM
FM	2.11	1.68	0.28	9.97	
FM_{RECON}	2.28	1.68	0.24	9.56	108.1
$(NH_4)_2SO_4$	0.62	0.39	0.09	2.65	29.4
NH_4NO_3	0.16	0.14	0.01	0.8	7.6
POM	0.98	0.93	0.03	6.98	46.4
LAC	0.08	0.07	0.01	0.57	3.8
SOIL	0.45	0.67	0.01	5.02	21.3
Sea salt	0	0	0	0.01	0.0
Brigantine Fine Mass	N = 114				
Variable (μg m^{-3})	Mean	Std. Dev.	Minimum	Maximum	% of FM
FM	9.74	5.79	3.43	35.06	
FM_{RECON}	10.18	5.87	3.66	29.8	104.5
$(NH_4)_2SO_4$	5.26	4.14	1.11	21.74	54.0
NH_4NO_3	1.07	1	0.18	5.23	11.0
POM	2.83	1.75	0.7	11.26	29.1
LAC	0.38	0.2	0.02	1.03	3.9
SOIL	0.55	0.43	0.03	1.94	5.6
Sea salt	0.09	0.36	0	2.13	0.9

Table 6.6. Statistical summary of annual coarse mass and coarse mass species concentrations by site.

Mount Rainier Coarse Mass	N = 114				
Variable (μg m^{-3})	Mean	Std. Dev.	Minimum	Maximum	% of CM
CM	2.84	2.13	0.11	8.25	
CM_{RECON}	2.97	2.43	-3.47	10.09	104.6
$(NH_4)_2SO_4$	0.07	0.12	-0.31	0.59	2.5
NH_4NO_3	0.1	0.14	-0.06	0.67	3.5
POM	1.68	1.81	-3.33	8.38	59.2
LAC	0.08	0.15	-0.41	0.64	2.8
SOIL	0.95	1.42	-0.02	6.09	33.5
Sea salt	0.08	0.16	0	0.78	2.8

San Gorgonio Coarse Mass	N = 116				
Variable (μg m^{-3})	Mean	Std. Dev.	Minimum	Maximum	% of CM
CM	6.95	5.57	0.15	25.55	
CM_{RECON}	6.2	4.76	-0.31	18.53	89.2
$(NH_4)_2SO_4$	-0.07	0.19	-0.88	0.28	-1.0
NH_4NO_3	0.74	0.73	-0.34	2.97	10.6
POM	0.96	0.99	-2.81	5.7	13.8
LAC	0.05	0.11	-0.14	0.54	0.7
SOIL	4.51	3.67	0	16.13	64.9
Sea salt	0.01	0.02	0	0.08	0.1
Sequoia Coarse Mass	N = 112				
Variable (μg m^{-3})	Mean	Std. Dev.	Minimum	Maximum	% of CM
CM	10.33	8.6	-1.75	33	
CM_{RECON}	12.39	10.81	0.24	40.61	119.9
$(NH_4)_2SO_4$	0	0.28	-1.07	0.56	0.0
NH_4NO_3	0.69	0.65	-1.72	2.75	6.7
POM	2.52	1.44	0.38	6.78	24.4
LAC	0.06	0.08	-0.14	0.47	0.6
SOIL	9.28	9.46	0.04	32.72	89.8
Sea salt	0.02	0.04	0	0.3	0.2
Grand Canyon Coarse Mass	N = 116				
Variable (μg m^{-3})	Mean	Std. Dev.	Minimum	Maximum	% of CM
CM	2.55	2.22	0.08	10.31	
CM_{RECON}	2.41	2.26	-1.91	10.54	94.5
$(NH_4)_2SO_4$	0.09	0.12	-0.25	0.52	3.5
NH_4NO_3	0.14	0.11	0	0.43	5.5
POM	0.22	0.55	-3.35	2.64	8.6
LAC	0.01	0.06	-0.24	0.23	0.4
SOIL	1.94	1.81	0.04	8.86	76.1
Sea salt	0.01	0.04	-0.02	0.32	0.4
Upper Buffalo Coarse Mass	N = 106				
Variable (μg m^{-3})	Mean	Std. Dev.	Minimum	Maximum	% of CM
CM	8.03	6.48	0.28	40.24	
CM_{RECON}	6.49	5.12	0.48	27.85	80.8
$(NH_4)_2SO_4$	0.21	0.48	-1.03	1.81	2.6
NH_4NO_3	0.51	0.42	-0.15	2.04	6.4
POM	1.64	0.97	-0.22	5.86	20.4
LAC	0.09	0.12	-0.54	0.47	1.1
SOIL	4.03	4.25	0.06	23.47	50.2
Sea salt	0.02	0.04	0	0.24	0.2

Bondville Coarse Mass	N = 102				
Variable (μg m^{-3})	Mean	Std. Dev.	Minimum	Maximum	% of CM
CM	5.77	5.86	-0.81	31.88	
CM_{RECON}	6.03	6.35	0	46.7	104.5
$(NH_4)_2SO_4$	0.13	0.58	-1.08	3.71	2.3
NH_4NO_3	0.42	0.36	-0.65	1.59	7.3
POM	1.85	2.09	0.02	15.29	32.1
LAC	0.17	0.24	-0.15	1.52	2.9
SOIL	3.45	5.14	0.11	39.73	59.8
Sea salt	0	0.02	-0.11	0.07	0.0
Great Smoky Mountains Coarse Mass	N = 112				
Variable (μg m^{-3})	Mean	Std. Dev.	Minimum	Maximum	% of CM
CM	3.37	2.7	0.26	14.97	
CM_{RECON}	3.01	2.44	-0.28	12.91	89.3
$(NH_4)_2SO_4$	0	0.77	-4.23	1.51	0.0
NH_4NO_3	0.39	0.41	-0.07	2.24	11.6
POM	1.36	1.06	-0.17	4.29	40.4
LAC	0.08	0.11	-0.18	0.48	2.4
SOIL	1.43	1.4	-0.01	9.12	42.4
Sea salt	0.01	0.06	0	0.59	0.3
Bridger Coarse Mass	N = 122				
Variable (μg m^{-3})	Mean	Std. Dev.	Minimum	Maximum	% of CM
CM	1.81	2.07	-0.01	12.73	
CM_{RECON}	1.99	2.24	-1.34	14.31	109.9
$(NH_4)_2SO_4$	0.1	0.13	-0.1	0.81	5.5
NH_4NO_3	0.11	0.15	-0.14	1.06	6.1
POM	0.42	0.57	-1.51	4.63	23.2
LAC	0.03	0.06	-0.45	0.18	1.7
SOIL	1.33	1.72	0	11.23	73.5
Sea salt	0	0.01	0	0.1	0.0
Brigantine Coarse Mass	N = 114				
Variable (μg m^{-3})	Mean	Std. Dev.	Minimum	Maximum	% of CM
CM	6.11	6.37	1.02	49.93	
CM_{RECON}	4.67	3.88	-0.69	27.81	76.4
$(NH_4)_2SO_4$	0.14	0.86	-1.82	4.54	2.3
NH_4NO_3	0.6	0.49	-0.08	2.33	9.8
POM	1.08	0.93	-1.44	4.49	17.7
LAC	0.05	0.15	-0.5	0.67	0.8
SOIL	2.06	2.49	-0.02	18.69	33.7
Sea salt	0.74	1.35	0	6.98	12.1

In general, the temporal variability, as well as composition of FM species collected during the year 2004, was similar to the grand average over all years. However, some differences are apparent. In most cases, FM concentrations during the year 2004 were generally less than the historical averages, perhaps reflecting the general reduction in species concentrations over the past 15 years (Malm et al., 2002). Sulfate concentrations have decreased across most of the United States, as have POM in the Northwest and nitrates in the coastal areas of California and inland at San Gorgonio wilderness area. Historical comparison at the Bondville site is less meaningful because routine monitoring was only initiated in the year 2001. At all monitoring sites, sulfates tend to be highest during the spring/summer/fall months when more sunlight is available and photochemistry is enhanced, while nitrates tend be highest during the cooler winter months. This is especially true at Bondville and Sequoia National Park where nitrates are 40–50+% of the FM from November to April. It interesting to note that at both Bondville and Upper Buffalo wilderness area fine mass concentrations tend to peak in February, then decrease, and peak again in late summer/fall months. Also, note the fine soil mass fraction (Fig. 6.25) increases during the month of April throughout most of the monitoring sites in the West and at Upper Buffalo. This trend is also observed at most IMPROVE monitoring sites in the western United States (Malm et al., 2002). Fine POM concentrations show less seasonal variability at the eastern sites, but show large seasonal variability at those sites representing the interior West, the Colorado plateau, and the Northwest. At Mount Rainier National Park, the ratio of POM in July to that in January is almost a factor of 10 (8.6).

Fig. 6.25 shows that reconstructed and gravimetric FM compare quite well, as reflected in Fig. 6.21. There are, however, a variety of reasons why these two variables should not agree. First, average molecular structure is assumed for all species, and this may be most important in the R_{oc} factor, which scales organic carbon to mass of carbon plus other elements that make up the organic mass concentration. In this analysis, $R_{oc} = 1.8$ was used. In the East, sulfates tend to be acidic during summer months and therefore retain water at RH values found in laboratories where filters are weighed and gravimetric mass concentrations derived (about RH = 40%). Therefore gravimetric mass reflects retained water, as well as the mass of the sulfate aerosol. Another potentially important artifact is the loss of ammonium nitrate from the Teflon substrate that is used for gravimetric analysis. Notice that, at Great Smoky Mountains National Park and Bondville, reconstructed mass is less than gravimetric mass during summer months, possibly reflecting retained water, while at San Gorgonio and Sequoia, where nitrates are a substantial fraction of FM, reconstructed mass is always higher than gravimetric mass, possibly reflecting loss of nitrate from the Teflon substrates. This is also true at some monitoring sites during the winter months, although one would expect that the nitrate loss artifact from Teflon filters would be lower because of lower ambient temperatures. At Mount Rainier and possibly Bridger and Sequoia, where POM is a significant fraction of FM and reconstructed mass is larger than gravimetric mass, the R_{oc} factor of 1.8 may be too high. In fact, an OLS regression with FM as the dependent variable and the species as independent variables suggests that the R_{oc} multiplier should be about 1.4 rather than the 1.8 used in this analysis.

Referring to Fig. 6.26 and Table 6.6, one can see that, for the most part, reconstructed and gravimetric CM compare quite favorably. This is also evident from Fig. 6.22, a scatter plot of reconstructed and gravimetric CM. However, it is evident from Fig. 6.22 that, although the data points scatter around the 1:1 line, there are a number of sampling periods where the two variables disagree by as much as a factor of 2.

It is clear that soil is the single largest contributor to CM at all but one monitoring location. The average fractional contributions range from a high of 76% at Grand Canyon National Park to a low of 34% at Mount Rainier. With the exception of Mount Rainier, the western United States generally has the highest fractional contributions, while the East has an average annual fractional contribution of 40–60%. The highest average concentration is found at Sequoia at 9.28 μg m^{-3}. Sequoia also has the highest average monthly contribution at near 21.5 μg m^{-3} for the month of August. San Gorgonio and Bondville have the second highest soil dust contributions at 4.5 and 3.5 μg m^{-3}, respectively, while Mount Rainier has the lowest average concentration of 0.95 μg m^{-3}.

Fig. 6.24 shows the lowest coarse soil concentrations tend to occur in the winter, as do most other species, while the months with maximum coarse soil contributions tend to vary from location to location. One interesting feature is the elevated soil concentrations during the month of April at Bondville and Upper Buffalo that are consistent with the historically high CM that occurs during this month. After this increase of CM in April, there is a decrease, followed by another increase in CM at Bondville and Upper Buffalo during the fall months. Whereas fine soil concentrations tend to peak across the entire western United States during the month of April, coarse soil concentrations do not show this trend. In the western United States, coarse soil concentrations tend to peak more toward mid-summer, and at Sequoia the highest concentrations are found in the fall.

The second largest contributor to CM is organic mass, which on an average annual fractional basis is highest at Mount Rainier at 59%. During the months of September and October, the fractional contribution of POM to CM was more than 80%. Even though POM contributes 59% of the CM on average at Mount Rainier, its average concentration is less than at the Sequoia and Bondville sites. The highest POM concentration occurs at Sequoia at 2.52 μg m^{-3} and the second highest at Bondville at 1.85 μg m^{-3}. At Great Smoky Mountains, organic mass contributes 40% on average, while at four sites organic mass concentrations contribute between 20% and 30% of the CM. The lowest fractional contribution of organic mass occurs at Grand Canyon and San Gorgonio.

Nitrates are on average the third largest contributor to CM concentrations. The highest fractional contributions to CM by nitrates are at Brigantine, Great Smoky Mountains, and San Gorgonio at 10–12%. However, at coastal sites such as Brigantine, nitrates may well be in the form of sodium nitrate resulting from reactions of nitric acid with sea salt. San Gorgonio and Sequoia actually have the highest coarse nitrate contributions at 0.74 and 0.69 μg m^{-3}, respectively. Brigantine is nearly as high at 0.6 μg m^{-3}. Whereas nitrates at coastal sites may be in the form of sodium nitrate, in the interior West they are more likely to be associated with soil elements such as calcium. As with fine nitrates, coarse nitrate concentrations tend to be highest during the winter months.

At most sites sea salt concentrations are very low, the one exception being Brigantine where the average concentration is 0.74 μg m^{-3} and is 12% of the CM budget. At Mount Rainier, sea salt contributes about 3% to the CM, and at the rest of the monitoring sites average concentrations are near 0.

Sulfates' contribution to CM is negligible on average at most sites, with its fractional contribution less than a few percent. This is also true on average for LAC.

It is interesting to contrast species mass concentrations that make up the fine and coarse modes. In the East, FM is dominated by sulfates, with organics contributing significantly less but in second place, while for CM soil is the biggest contributor, with organic mass again being in second place. In most of the rest of the United States, FM is made up of about equal amounts of sulfates, organics, and soil, with organics being the more significant contributor in the northwestern United States. Nitrates contribute little to FM except in southern California and the Midwest. In the coarse mode, soil is almost always the most significant fraction of mass, with organics being a distant second at about 24%. Other species on average are less than 10%.

6.4.6 Summary

To more fully investigate the composition of coarse particles, a nine-station coarse particle speciation network was initiated on 19 March 2003 and was completely operational by 23 December 2003. Sites were selected to be representative of the continental United States and were operated according to IMPROVE protocols for the year 2004. Both $PM_{2.5}$ (FM) and PM_{10} ($CM = PM_{10}–PM_{2.5}$) mass concentrations were speciated for sulfates, nitrates, organic and light-absorbing carbon, crustal minerals (soil), and sea salt. For FM, the sum of species mass concentrations values was 7% greater than gravimetric on average, while for CM the sum was 3% less than gravimetric mass on average. Scatter plots of reconstructed FM and CM versus gravimetric FM and CM show OLS slopes with the intercept set equal to 0 to be $1.03 \pm .004$ and $0.95 \pm .01$, respectively.

On average for the nine monitoring sites, sulfate (interpreted as ammonium sulfate) and POM make up 41% and 35% of the FM, respectively, while ammonium nitrate contributes another 18%. Soil mass concentration is less than 10% of measured mass, LAC about 4%, and sea salt is negligible.

For the CM fraction, the sulfate contribution is negligible, and LAC and sea salt are only 1% and 2%, respectively. As expected, soil is the major component at 61%, but POM and ammonium nitrate contribute significantly at 24% and 8%, respectively. The average fractional contributions of soil to CM range from a high of 76% at Grand Canyon to a low of 34% at Mount Rainier. With the exception of Mount Rainier, the western United States generally has the highest fractional contributions, while the East has an average annual fractional contribution of 40–60%. The lowest soil concentrations tend to occur in the winter, as do most other species, while the months with maximum soil contributions tend to vary from location to location.

The second largest contributor to CM is organic carbon mass, which on an average annual fractional basis is highest at Mount Rainier at 59%. During the months of September and October, the fractional contribution of POM to CM was more than 80%. The lowest fractional contribution of organic mass occurs at Grand Canyon and San Gorgonio.

Nitrates are on average the third largest contributor to CM concentrations. The highest fractional contributions to CM by nitrates are at Brigantine, Great Smoky Mountains, and San Gorgonio at 10–12%. However, at coastal sites such as Brigantine, nitrates may well be in the

form of sodium nitrate, which results from reactions of nitric acid with sea salt. Whereas nitrates at coastal sites may be in the form of sodium nitrate, in the interior West they are more likely to be associated with soil elements such as calcium. As with fine nitrates, coarse nitrate concentrations tend to be highest during the winter months.

At most sites sea salt concentrations are very low, the one exception being Brigantine where the average contribution to CM is 12%. At Mount Rainier, sea salt contributes about 3% to the CM, and at the rest of the monitoring sites average concentrations are near 0. Sulfates' contribution to CM is negligible on average at most sites, with its fractional contribution less than a few percent. This is also true on average for LAC.

Disclaimer

The assumptions, findings, conclusions, judgments, and views presented herein are those of the authors and should not be interpreted as necessarily representing the National Park Service or the National Oceanic and Atmospheric Administration policies.

References

Chow J.C., Watson J.G., Pritchett L.C., Pierson W.R., Frazier C.A., Purcell R.G., 1993. The DRI thermal/optical reflectance carbon analysis system: Description, evaluation, & applications in U.S. air quality studies. Atmospheric Environment 27A, 1185-1201.

Eldred R.A., Cahill T.A., Pitchford M., Malm W.C., 1988. IMPROVE - A new remote area particulate monitoring system for visibility studies. Presented at the 81st Annual Meeting of the Air Pollution Control Association, Dallas.

Eldred R.A., Cahill T.A., Malm W.C., Pitchford M.L., 1993. Ten-year trends in sulfur concentrations at national parks throughout the United States. Presented at the 86th Annual Meeting of the Air & Waste Management Association, Denver.

Eldred R.A., 1997. Comparison of selenium and sulfur at remote sites throughout the United States. Journal of the Air & Waste Management Association 47, 204-211.

Gebhart K.A., Malm W.C., Day D., 1994. Examination of the effects of sulfate acidity & relative humidity on light scattering at Shenandoah National Park. Atmospheric Environment 28, 841-849.

Iyer H., Patterson P., Malm W.C., Delgado J., 2000. Trends in the extremes of sulfur concentration distributions. Journal of the Air & Waste Management Association 50, 802-808.

Joseph D., Metza B.J., Malm W.C., Pitchford M.L., 1987. A Federal Program to Monitor Visibility in Class I Areas; in: Bhardwaja P.J. (Ed.), Visibility Protection: Research and Policy Aspects, Air Pollution Control Association, Pittsburgh.

Lee T., Kreidenweis S.M., Collett J.L. Jr., 2004. Aerosol ion characteristics during the Big Bend Regional Aerosol and Visibility Observational Study. Journal of the Air & Waste Management Association 54, 585-592.

Lefer B.L., Talbot R.W., 2001. Summertime measurements of aerosol nitrate and ammonium at a northeastern U.S. site. Journal of Geophysical Research 106, 20365-20378.

Malm W.C., Gebhart K.A., Latimer D., Cahill T.A., Eldred R., Pielke R., Stocker R.A., Watson J.G., 1989. National Park Service Report on the Winter Haze Intensive Tracer Experiment, Final Report.

Malm W.C., Sisler J.F., Huffman D., Eldred R.A., Cahill T.A., 1994. Spatial and seasonal trends in particle concentration and optical extinction in the U.S. Journal of Geophysical Research 99, 1347-1370.

Malm W.C., Day D.E., 2000. Optical properties of aerosols at Grand Canyon National Park. Atmospheric Environment 34, 3373-3391.

Malm W.C., Sisler J.F., 2000. Spatial patterns of major aerosol species and selected heavy metals in the United States. Fuel Processing Technology 65, 473-501.

Malm W.C., Sisler J.F., Pitchford M.L., Scruggs M., Ames R., Copeland S., Gebhart K.A., Day D.E., 2000a. IMPROVE (Interagency Monitoring of Protected Visual Environments): Spatial and Seasonal Patterns and Temporal Variability of Haze and Its Constituents in the United States: Report III; CIRA Report ISSN: 0737-5352-47, Colorado State University, Fort Collins, CO.

Malm W.C., Day D.E., Kreidenweis S.M., 2000b. Light scattering characteristics of aerosols as a function of relative humidity: Part I: A comparison of measured scattering and aerosol concentrations using the theoretical models. Journal of the Air & Waste Management Association 50, 686-700.

Malm W.C., Schichtel B.A., Ames R.B., Gebhart K.A., 2002. A ten-year spatial and temporal trend of sulfate across the United States. Journal of Geophysical Research 107, doi:10.1029/2002JD002107.

Malm W.C., Day D.E., Kreidenweis S.M., Collett J.L., Lee T., 2003. Humidity-dependent optical properties of fine particles during the Big Bend Regional Aerosol and Visibility Observational Study. Journal of Geophysical Research 108, doi:10.1029/2002JD002998.

Malm W.C., Schichtel B.A., Pitchford M.L., Ashbaugh L.L., Eldred R.A., 2004. Spatial and monthly trends in speciated fine particle concentration in the United States. Journal of Geophysical Research 109, doi:10.1029/2003JD003739.

Malm W.C., Day D.E., Carrico C.A., Kreidenweis S.M., Collett J. Jr., McMeeking G., Lee T., Carrillo J., Schichtel, B.A., 2005. Intercomparison and closure calculations using measurements of aerosol species and optical properties during the Yosemite Aerosol Characterization Study. Journal of Geophysical Research 10, doi:10.1029/2004JD005494.

Malm W.C., Hand J.L., 2006. Mass scattering and extinction efficiencies derived from aerosol composition data using linear regression techniques. In preparation.

Patterson P., Iyer H.K., Sisler J.F., Malm W.C., 2000. An analysis of the yearly changes in sulfur concentrations at various national parks in the United States. Journal of the Air & Waste Management Association 50, 790-201.

Poirot R.L., R.B.Husar, 2004. Chemical and physical characteristics of wood smoke in the northeastern U.S. during July 2002: Impacts from Quebec forest fires. Paper # 94, Air and Waste Management Association Specialty Conference: Regional and Global Perspectives on Haze: Causes, Consequences and Controversies, Asheville, NC, October 25-29.

Quinn P.K., Coffman D.J., Bates T.S., Miller T.L., Johnson J.E., Voss K., Welton E.J., Neususs C., 2001. Dominant aerosol chemical components and their contribution to extinction during the Aerosols99 cruise across the Atlantic. Journal of Geophysical Research 106(D18), 20783-20809.

Seinfeld J.H., Pandis S.N., 1998. Atmospheric Chemistry and Physics: From Air Pollution to Climate Change, John Wiley, New York, p. 444.

Sisler J.F., Huffman D., Latimer D.A., 1993. Spatial and Temporal Patterns and the Chemical Composition of the Haze in the U.S.: An Analysis of Data from the IMPROVE Network, 1988-1991; CIRA Report ISSN 0737 5352 26, Colorado State University, Fort Collins, CO.

Sisler J.F., Malm W.C., 2000. Interpretation of trends of PM2.5 and reconstructed visibility from the IMPROVE network. Journal of the Air & Waste Management Association 50, 775-789.

Turpin B.J., Lim H.J., 2001. Species contributions to $PM_{2.5}$ mass concentrations: Revisiting common assumptions for estimating organic mass. Aerosol Science and Technology 35, 602-610.

U.S. Environmental Protection Agency, 1999. Regional Haze Regulations: Final Rule. 40 CFR Part 51, 64(126), Docket No. A-95-38, Federal Register.

White W.H., Eldred R.A., Feeney P.J., McDade C.E., Perley B.P., Shadoan D.J., Wakabayashi P.H., 2004. Behavior of fine-particle elemental data near the detection limit. Paper # 24, Air and Waste Management Association Specialty Conference: Regional and Global Perspectives on Haze: Causes, Consequences and Controversies, Asheville, NC, October 25-29.

Figure 6.21. Scatter plot of gravimetric and reconstructed fine mass. An ordinary least square slope with the intercept set equal to 0 is 1.03 ± 0.004 with an $R^2 = 96$.

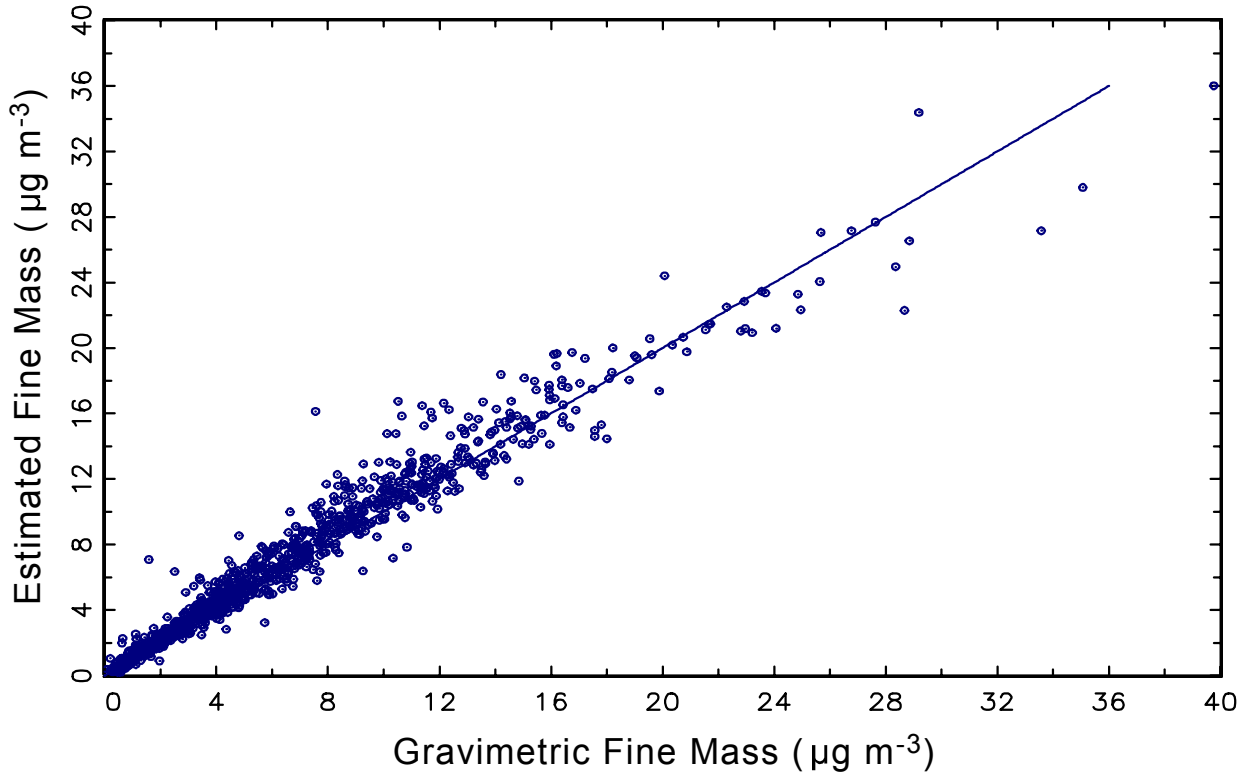

Figure 6.22. Scatter plot of gravimetric and reconstructed coarse mass. An ordinary least square slope with the intercept set equal to 0 is 0.95 ± 0.01 with an $R^2 = 81$.

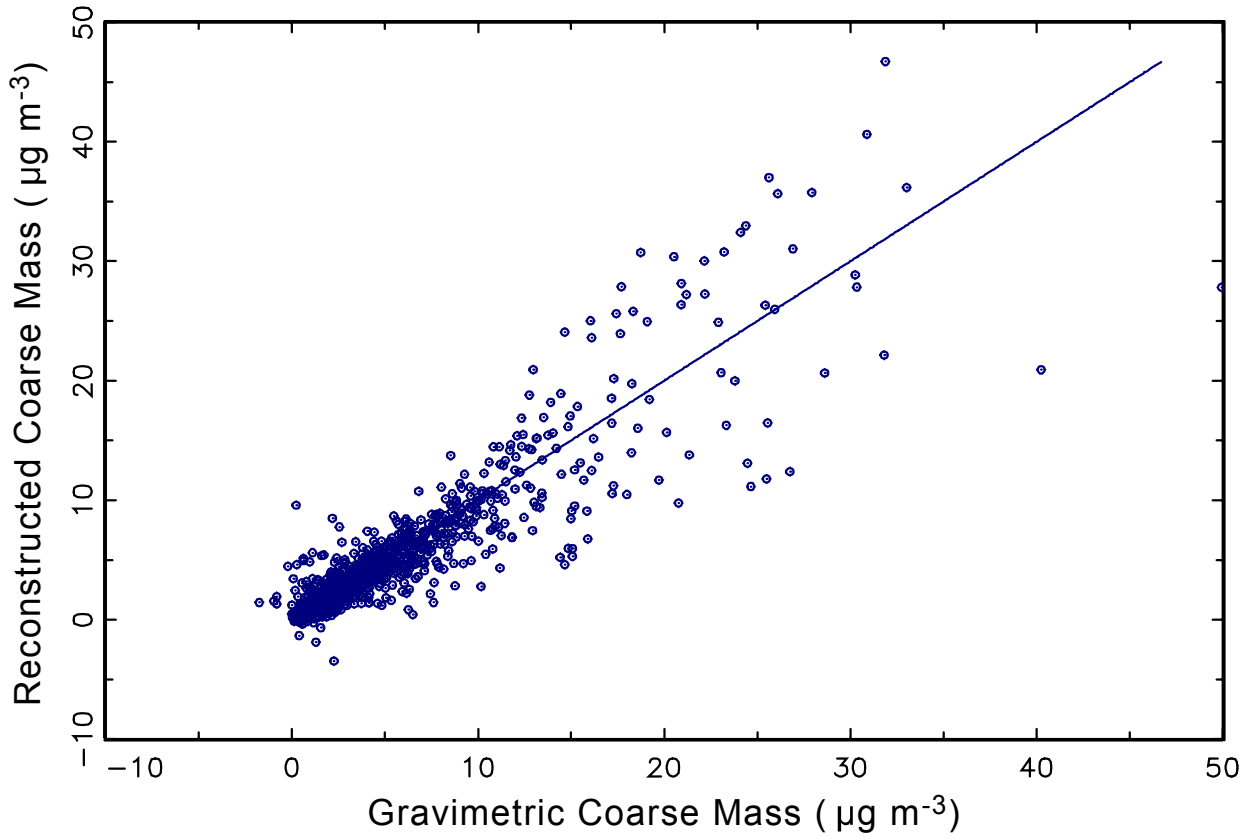

Figure 6.23. A map of stacked bar charts showing the fine mass concentration of each species at each of the nine locations at which measurements were made. The continuous lines are running averages of the data collected historically at each monitoring site.

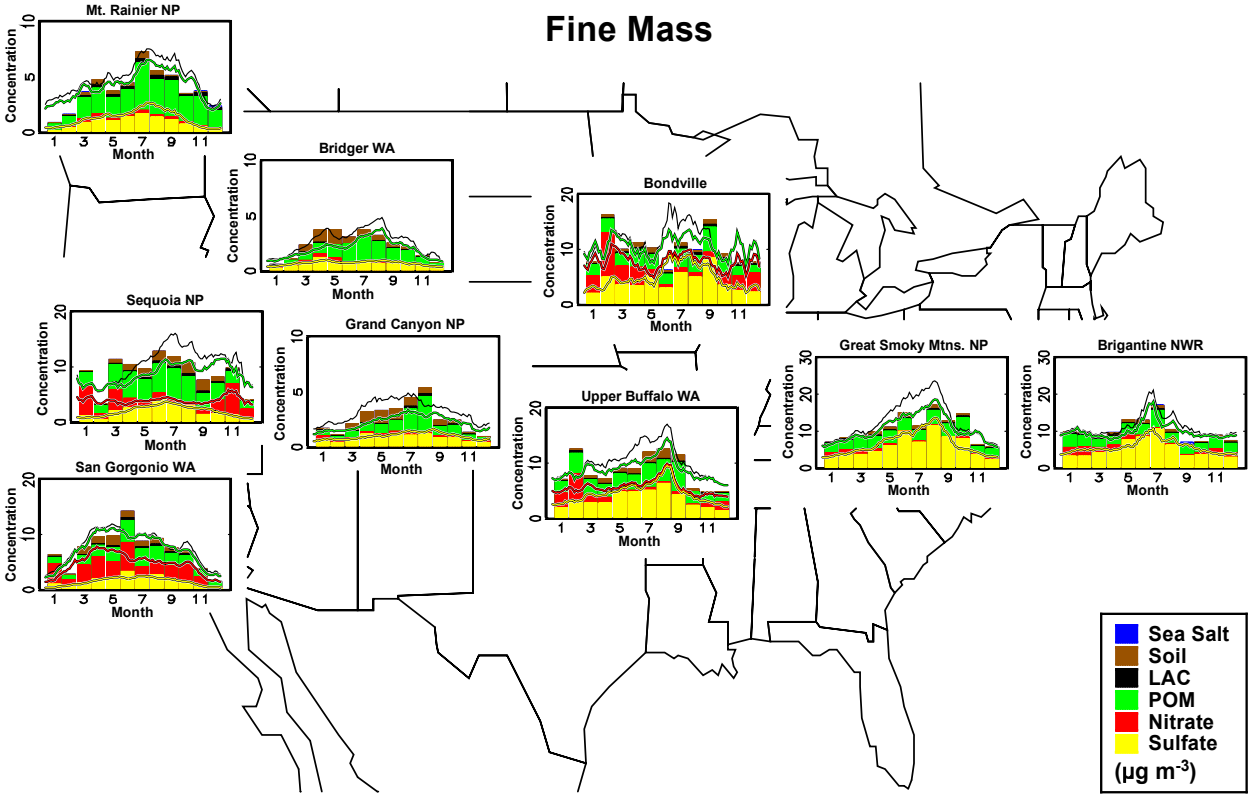

Figure 6.24. A map of stacked bar charts showing the coarse mass concentration of each species at each of the nine locations at which measurements were made. The continuous lines are running averages of the data collected historically at each monitoring site.

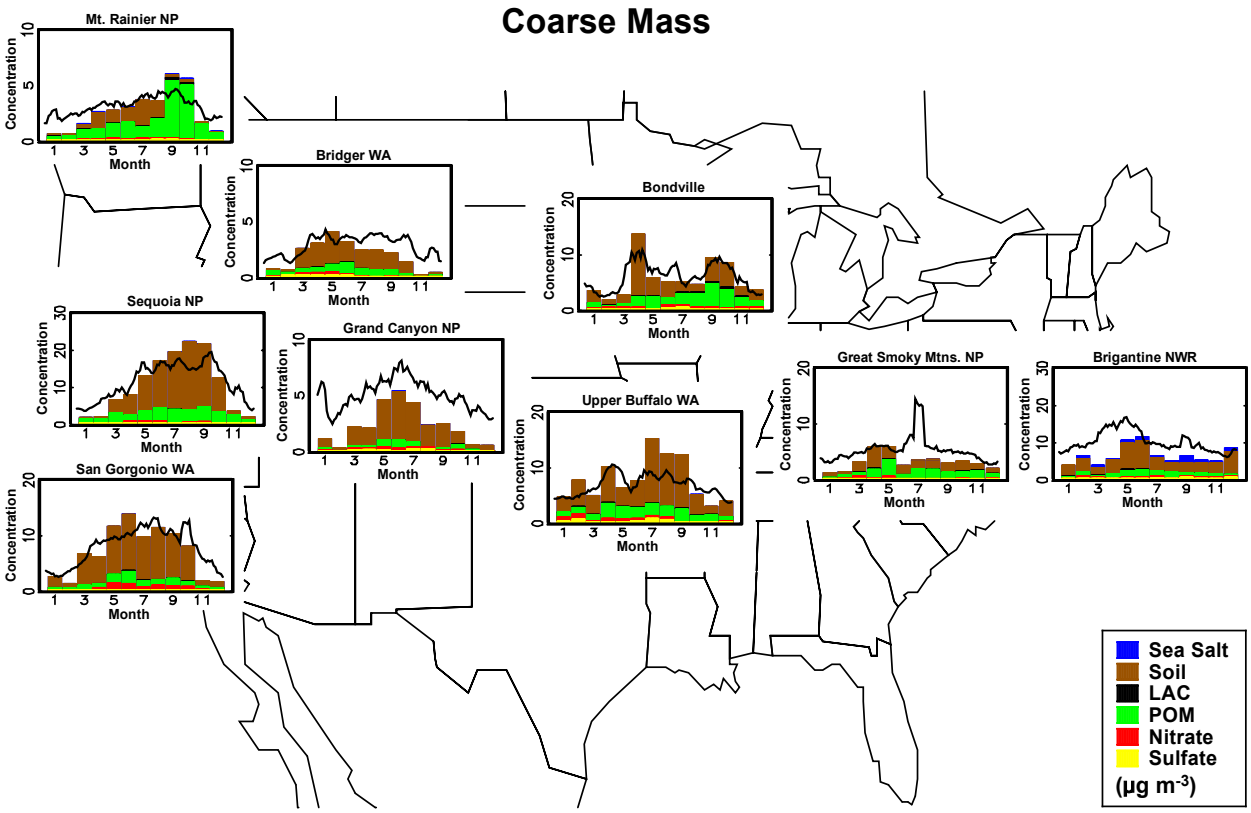

Figure 6.25. A map of stacked bar charts showing the fractional contribution of each fine mass species to gravimetric mass at each of the nine locations at which measurements were made.

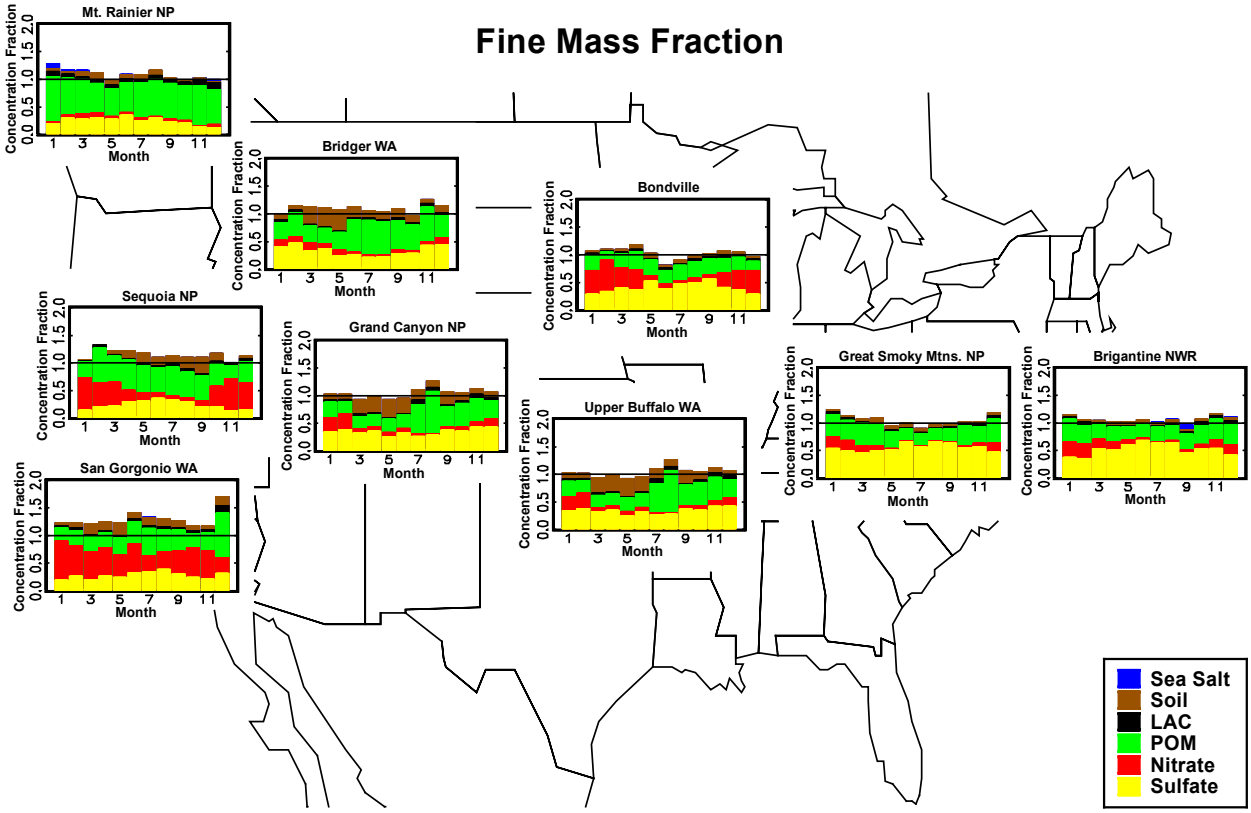

Figure 6.26. A map of stacked bar charts showing the fractional contribution of each coarse mass species to gravimetric mass at each of the nine locations at which measurements were made. The stacked bar chart for the month of January is not shown for Sequoia National Park because of a large uncertainty in PM_{10} gravimetric mass.

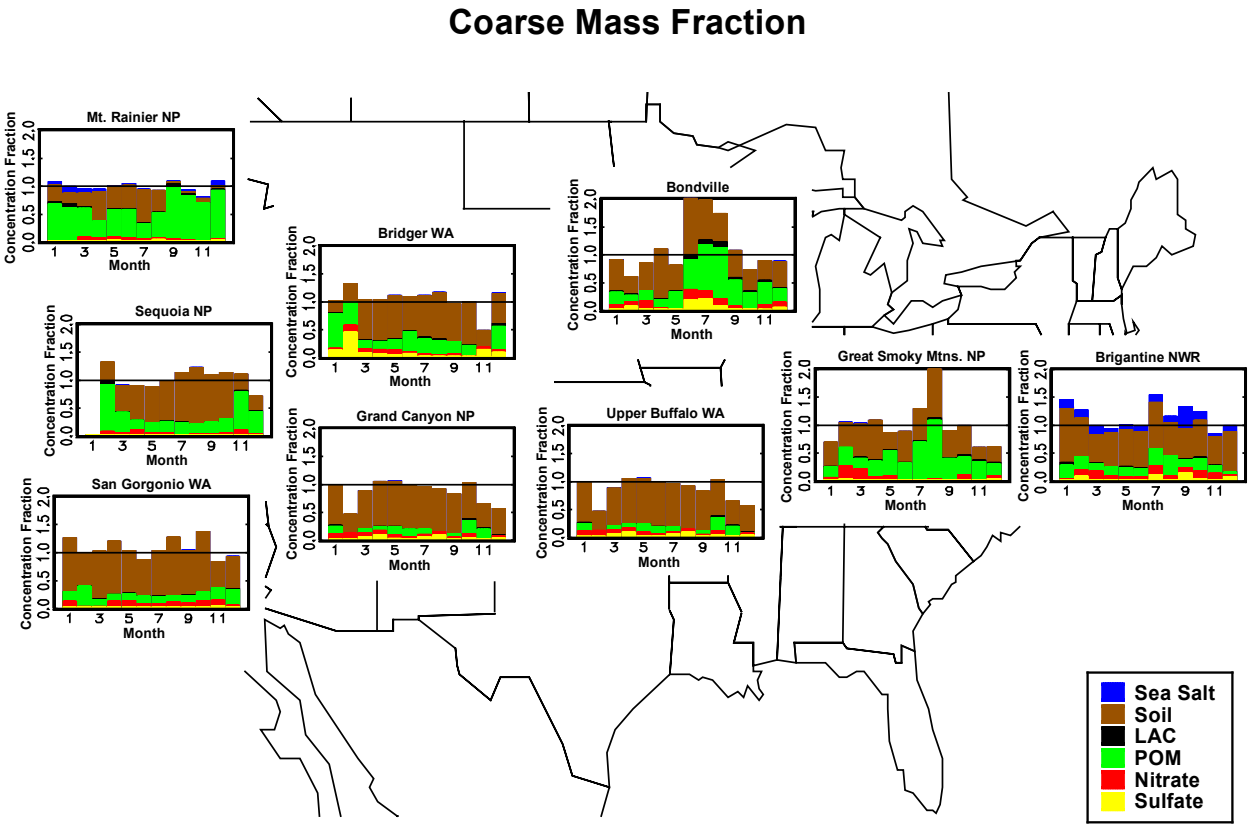

6.5 THE COMPARABILITY OF IMPROVE AND STN MEASUREMENTS—A SUMMARY OF THE RESULTS AND CONCLUSIONS FROM AN ANALYSIS OF COLLOCATED MEASUREMENTS DETAILED IN APPENDIX E

The $PM_{2.5}$ chemical Speciation Trends Network (STN) also monitors speciated fine aerosol mass concentrations at ~300 sites located primarily in urban and suburban areas, in contrast to IMPROVE, which has sites located primarily in remote rural locations. The STN was established in a manner such that it has similar measurements to those collected by IMPROVE—both networks collect 24-hour samples on appropriate filter media on a 1-in-3-day sampling schedule for quantifying $PM_{2.5}$ mass and its chemical constituents. The collocation of IMPROVE and STN sites in select urban and rural locations allows for analysis of the intercomparability between the two monitoring networks. Measurements from collocated IMPROVE and STN sites are expected to be the same within combined measurement uncertainty for most parameters. IMPROVE and STN utilize gravimetric analysis for quantification of $PM_{2.5}$ mass, IC for NO_3^- and $SO_4^=$, and XRF for elements including S, Al, Fe, Ca, Si, and Ti. However, the two networks use different samplers and different standard operating procedures for sample collection and analysis and maintain independent quality assurance programs.

Integrating data from the two networks provides more complete information on the spatial and temporal distributions of $PM_{2.5}$ aerosol mass and its major constituents throughout the United States. The in-network collocated data from IMPROVE and STN, as well as the cross-network collocated data, were explored to develop estimates on the comparability of multiyear mean concentrations between sites from the two networks. The purpose of this analysis was to provide an adequate framework for the spatial and temporal trends examined in Chapters 2 and 3 using data from both the IMPROVE and STN networks. The details of this study including data set descriptions, statistical methodology, and detailed results are given in Appendix E of this report.

The goal of these analyses was to answer the question, from a usability stand point, how comparable are the IMPROVE and STN data? The specific arena this study aimed to address is the comparability of collocated multiyear mean concentrations for each of the measurements utilized in the IMPROVE RCFM model, calculated utilizing all reported concentration values. Paired mean values were composed of between 4 months and 2+ years of data, depending on the length of the available data record; the IMPROVE-STN collocated samplers all had record lengths of at least 1 year and generally 2+ years.

The IMPROVE in-network collocated data were examined to 1) determine if the observed relative measurement errors were consistent with idealized random errors and 2) establish the typical uncertainty in mean concentrations calculated from the collocated IMPROVE measurements. The discussion of the in-network IMPROVE collocated data was included to provide context for analysis of the cross-network collocated data. The cross-network IMPROVE and STN collocated data were explored with the same objectives as the in-network IMPROVE collocated data, with appropriate statistical modifications to account for the expected differences in measurement errors between the two networks. Finally, the characteristic uncertainties observed in the in-network IMPROVE and in-network STN collocated data were used to calculate the expected characteristic uncertainties in the cross-network collocated data. The objective of this step was to evaluate the observed cross-network measurement uncertainty

in the context of what we would expect if the only information we had was the uncertainties observed in the individual networks.

The combined analysis of the in-network and cross-network collocated data populations led to a number of important conclusions regarding the observed measurement errors and the comparability of mean concentrations within and between IMPROVE and STN:

1. Biases between the IMPROVE and STN measurements of the soil elements and OC are readily apparent in the analysis of the cross-network collocated data. In the case of the soil elements, the biases are indicated by low R^2 values (<0.55) in the correlation analysis and median relative errors greater than 0. IMPROVE routinely reports higher values for the soil elements as compared to STN. The biases in OC were in the opposite direction; the median relative difference was less than 0, indicating that IMPROVE was consistently reporting lower OC values than STN. The bias observed in the OC measurements is consistent with only the IMPROVE measurements being blank corrected.

2. There are errors present in the IMPROVE and/or STN measurements that are identified in the IMPROVE-STN collocated data that are not apparent in the IMPROVE-IMPROVE or STN-STN collocated data. These additional errors are identified by larger than expected observed root mean square (rms) relative differences. The expectations were based upon simple propagation of error techniques, whereby the expected rms relative difference in the cross-network collocated data is the square root of the sum of the squared relative precision observed in each network's in-network collocated data. The observed rms relative differences observed in the IMPROVE-STN collocated data were 15–50 percentage points higher than expectations for all parameters besides S and SO_4. Analysis of cross-network collocated data identifies previously hidden errors, particularly measurement biases, which for most parameters are of considerable magnitude.

3. The analysis of the in-network IMPROVE collocated data revealed that there are nonrandom errors present in the IMPROVE measurements that are identified by larger than expected observed relative differences in the paired mean values. The expectations were based on the model of random errors, whereby independent random errors will "cancel each other out" as the sample size of the average value increases at the rate of $1/\sqrt{n}$. The parameters that had multiple aggregates with observed relative errors in the paired means more than 3 standard deviations away from expectations were SO_4, OC, Al, and Ca. These results suggest that, for these parameters, nonrandom errors (biases) are present such that the characteristic relative error for the parameter does not provide a meaningful estimate of the errors in the mean value under independent and identically distributed (i.i.d.) assumptions. This does not necessarily imply that the characteristic relative error for the parameter is too low; rather it could be that the assumption of completely independent measurement errors is incorrect. For example, a significant flow bias related to an annual calibration in one of the collocated samplers is not independent for each 24-hour sampling period during that year.

4. The IMPROVE measurement errors are inconsistent with idealized random errors—they are not i.i.d. nor are they Gaussian when the entire population is examined. Thus data analysts must be cautious in their use of any statistical techniques that require an assumption of i.i.d. or normal errors.

    a. There are significant nonrandom errors (biases) present in several of the IMPROVE measurements (see conclusion 4) that additionally are likely shared (dependent) among certain subsets of measurements. Sampling errors seem like the probable source for the biases between the collocated IMPROVE measurements, given that they were all analyzed batch-wise so that the analytical conditions should have been very similar.

    b. The IMPROVE measurement errors are heteroscedastic—they show significant relationships with both time and concentration in terms of central tendency and variability, indicating that the distribution of the errors is not the same for the entire sample population. Heteroscedastic measurement errors are expected when the measurement process spans concentrations from below minimum detection limits (mdl) to those that are well quantified. However, many statistical techniques are highly sensitive to heteroscedastic errors and require the data analyst to either pretreat the data by transforming the data to equalize the errors or to select robust techniques.

    c. The IMPROVE measurement errors do not follow a single normal distribution and for many parameters do not follow a single symmetrical distribution. This does not necessarily indicate that the error distribution at any fixed concentration is not Gaussian. For example, the high concentrations could all have errors drawn from a normal distribution with mean value $\mu = 0$ and standard deviation σ_1, $N(0, \sigma_1)$, and the lower concentrations have their errors drawn from a normal distribution with the same mean value and a larger standard deviation, $N(0, \sigma_2)$, where $\sigma_1 < \sigma_2$ and the result of grouping all these samples together would be a nonnormal error distribution.

5. The combined measurement errors observed in the cross-network collocated are additionally inconsistent with idealized i.i.d random errors in that they are heteroscedastic and as a whole nonnormal. As no analysis of the in-network STN collocated data was done, it is not possible to determine if this is just a result of IMPROVE having heteroscedastic measurement errors or if STN measurements exhibit the same inconsistencies. The same cautions, about applying statistics requiring i.i.d. or normal errors, apply to any joint analysis of the IMPROVE and STN data.